ACIBADEM MEHMET ALI AYDINLAR UNIVERSITY
INSTITUTE OF HEALTH SCIENCES

INVESTIGATION OF GENETIC CAUSATION UNDERLYING MICROLISSENCEPHALY SPECTRUM OF DISORDERS

MELİSA ARAL

M.Sc. THESIS

DEPARTMENT OF GENOME STUDIES

SUPERVISOR
Asst. Prof. Kaya Bilgüvar

ISTANBUL-2025

ACIBADEM MEHMET ALI AYDINLAR UNIVERSITY
INSTITUTE OF HEALTH SCIENCES

INVESTIGATION OF GENETIC CAUSATION UNDERLYING MICROLISSENCEPHALY SPECTRUM OF DISORDERS

MELİSA ARAL

M.Sc. THESIS

DEPARTMENT OF GENOME STUDIES

SUPERVISOR
Asst. Prof. Kaya Bilgüvar

ISTANBUL-2025

DECLARATION

I declare that this thesis work is my own work, I had no unethical behavior at any stages from the planning to the writing of the thesis, I obtained all the information in this thesis in accordance with academic and ethicel rules, I cited all the information and comments that were not obtained with this thesis work, and I provided resources in the list of references. I also declare that there was no violation of any patents and copyrights during the study and writing of this thesis.

10/07/2025
Melisa Aral

PREFACE AND ACKNOWLEDGEMENT

This study was supported by Acibadem University and the Yale Program on Neurogenetics, and the National Institutes of Health (NIH) grants RC2 NS070477 and R01 MH103616. My sincere thanks go to the affected individuals and their families for making this study possible through their valuable contributions.

There are certain milestones in life that shape who we become. During my master's degree, one of the most meaningful milestones for me was beginning to work with you, Dr. Kaya Bilgüvar. This thesis is far from being just my own work; it carries the imprint of your never-ending support and care. Your mentorship was not only a guide but also a constant driving force for me to grow into the best version of myself; thank you for that.

I am deeply appreciative of A. Gülhan Ercan-Şençiçek, PhD, for her countless efforts and assistance from overseas. I am also grateful to Prof. A. Okay Çağlayan for his involvement in ensuring patient contact on the clinical side to the extent possible.

I feel honored by all that I have learned from Genome Studies academics and their formative discussions.

I also owe a debt of gratitude to my friends, with whom I have shared so many experiences over the past two years. I'm truly glad to have met you.

My heartfelt thanks go to everyone who witnessed my complaints during the MSc period, who remained patient even when my stress levels stressed you out, and whose names I cannot mention one by one. What a roller coaster ride it has been!

But my deepest gratitude goes to my dear parents and my sister for their generous understanding, which has allowed me to grow professionally, as in every other part of my life. I feel incredibly lucky to have you by my side in all matters.

TABLE OF CONTENTS

ABBREVIATIONS AND SYMBOLS

CNV	Copy Number Variation
CP	Cortical Plate
FCD	Focal Cortical Dysplasia
IBC	Inbreeding Coefficient
IKNM	Interkinetic Nuclear Migration
ILS	Isolated Lissencephaly Sequence
IP	Intermediate Progenitor
MCD	Malformations of Cortical Development
MCPH	Microcephaly Primary Hereditary
MDS	Miller-Dieker Syndrome
MLIS	Microlissencephaly
MST	Mitotic Somal Translocation
NDD	Neurodevelopmental Disorders
NESC	Neuroepithelial Stem Cell
NPC	Neural Progenitor Cell
oRG	Outer Radial Glia
PNH	Periventricular Nodular Heterotopia
SVZ	Subventricular Zone
vRG	Ventricular Radial Glia
VZ	Ventricular Zone
WES	Whole Exome Sequencing
WGS	Whole Genome Sequencing

LIST OF FIGURES

LIST OF TABLES

ABSTRACT

Investigation of Genetic Causation Underlying Microlissencephaly Spectrum of Disorders

Marked by considerable heterogeneity, the microlissencephaly (MLIS) group of disorders reflects a broad phenotypic spectrum, frequently manifesting alongside other cortical malformations and exhibiting variable inheritance patterns, clinical severity, and associated syndromic features. Despite their low prevalence within the neurodevelopmental disorder (NDD) population, these conditions are often severe and demand a deep dive into the genome to be elucidated. The utilization of whole-exome sequencing (WES) technology has enabled the identification of disease-causing variants that previously went unrecognized. In this study, in-house exome sequencing data from nine unrelated Turkish patients with MLIS were analyzed. Syndromic MLIS cases were evaluated through both small-scale variant (SNV/indel) and structural variant (CNV/SV) analyses, and for cases with unexplained etiology, further gene/pathway-level analyses were conducted. Our findings revealed pathogenic variants in known MLIS-associated genes in six patients, while in the remaining three, novel candidate genes were identified that may underlie plausible biological mechanisms linked to critical pathways involved in neuronal development. Addressing these gaps in MLIS, as in other rare disorders, represents an important direction of research toward a deeper understanding of the mechanisms underlying such complex conditions.

Keywords: Microlissencephaly, Neurodevelopmental disorders, Rare diseases, Variant interpretation, Whole-exome sequencing

ÖZET

Mikrolizensefali Bozukluklarının Altında Yatan Genetik Nedenselliğin Araştırılması

Önemli ölçüde heterojenlik gösteren mikrolizensefali (MLIS) bozuklukları, sıklıkla diğer kortikal malformasyonlarla birlikte ortaya çıkan, değişken kalıtım kalıpları, klinik şiddet düzeyleri ve ilişkili sendromik özellikler sergileyen geniş bir fenotipik spektrumu sunar. Nörogelişimsel bozukluklar (NDD) popülasyonunda düşük prevalansa sahip olmalarına rağmen, bu bozukluklar genellikle ağır seyirlidir ve açıklığa kavuşturulmaları için genom düzeyinde derinlemesine analiz gerektirir. Tüm ekzom dizileme (WES) teknolojisinin kullanımı, daha önce tanımlanamamış hastalık etkeni varyantların tespit edilmesini mümkün kılmıştır. Bu çalışmada, akraba olmayan dokuz Türk mikrolizensefali hastasının ekzom dizileme verileri analiz edilmiştir. Hem küçük ölçekli varyantlar (SNV/indel) hem de yapısal varyant (CNV/SV) analizleri ile sendromik MLIS vakaları değerlendirilmiş, etiyolojisi açıklanamayan olgular için ise gen ve yolak düzeyinde ileri analizler gerçekleştirilmiştir. Bulgularımız, dokuz hastanın altısında hastalıkla ilişkilendirilmiş MLIS genlerinde patojenik varyantlar tanımlarken; geri kalan üç olguda ise klasik analizlerle açıklanamayan, nöronal gelişim süreçlerinde rol oynayan kritik yolaklarla ilişkili olabilecek yeni aday gen varyantlarına bağlı muhtemel biyolojik mekanizmaların anlaşılmasına katkı sağlamıştır. Diğer nadir hastalıkların yanı sıra, MLIS için bu bilgi boşluklarının giderilmesi, bu karmaşık durumların altında yatan mekanizmaları daha iyi kavramaya yönelik önemli bir araştırma alanı olarak değerlendirilmektedir..

Anahtar Sözcükler: Mikrolizensefali, Nörogelişimsel bozukluklar, Nadir hastalıklar, Varyant yorumlama, Tüm ekzom dizileme

1 INTRODUCTION AND AIM

Malformations of cortical development (MCD) are increasingly acknowledged as key contributors to neurodevelopmental disorders (NDD), including epileptic seizures, intellectual disability and potentially autism spectrum disorders (1). A substantial proportion of these malformations have a critical need for comprehensive genetic counseling in affected families.

The relationship between genotype and phenotype is often nonlinear, complicating efforts to draw direct correlations between genetic variation and clinical presentation. Even when a pathogenic variant is identified, considerable phenotypic heterogeneity can pose significant challenges for diagnosis and clinical management. Individuals carrying the same disease-causing mutation, such as siblings, may present with strikingly different clinical phenotypes. These cases often reflect the complexity of rare disease penetrance and expressivity and may represent patients who have remained undiagnosed despite undergoing extensive genetic testing, including previous reliance on Sanger sequencing methods.

In current medical genetics practice, whole-exome sequencing (WES) has become a standard tool due to its capacity to detect not only single nucleotide variants but also copy number variations (CNV) and certain non-coding alterations (2). While these types of investigations may be regarded as a preliminary phase, they could aid in clarifying the etiology of various NDD cases for which a precise diagnosis remains unattainable. This complexity is, in part, driven by genetic interactions and the influence of genetic modifiers, secondary variants that can modulate the phenotypic outcome of a primary pathogenic mutation. Such modifiers contribute to the broad spectrum of clinical variability observed in many NDDs (3).

Research into complex brain disorders has led to the identification of numerous genes that play critical roles in key developmental processes, including neuronal migration, cortical folding (gyrification), and overall brain growth (4). Importantly, the integration of genomic data with experimental models based on patient-derived

cells offers a powerful approach to uncovering the intricate regulatory networks involved. Such combined strategies provide a deeper understanding of the molecular architecture underlying brain development and facilitate the dissection of complex disease mechanisms.

The identification of causative genes underlying NDDs, followed by in-depth functional characterization of these genes, represents a critical step toward a more comprehensive understanding of human brain development. Nevertheless, our current knowledge of the molecular mechanisms governing cortical formation remains incomplete, and it is evident that a number of genes implicated in cortical malformations have yet to be discovered.

In this context, MLIS remain an especially enigmatic subgroup of cortical malformations, rare and severe NDDs that continue to pose significant challenges to both diagnosis and mechanistic understanding. These disorders are regarded as complex puzzles that have long resisted resolution (5).

In parallel with the rapid progress in gene discovery for developmental brain disorders and the emerging framework of genetic regulatory networks, we seek to explore the multifaceted and heterogeneous etiology of MLIS. Despite its rarity and the considerable diagnostic limitations it presents, elucidating the genetic architecture of this disorder is essential for overcoming barriers in the path toward accurate and timely molecular diagnoses in neurodevelopmental conditions.

With this perspective, our objective is to systematically characterize known MLIS-associated genes while also investigating the distribution of pathogenic variants in novel candidate genes. By leveraging biological network analysis, we aim to map these genes within broader regulatory modules, thereby expanding the current understanding of the genetic etiology of MLIS.

2 BACKGROUND

2.1 Early Cortical Development

2.1.1 Neurogenesis: cellular foundation of the cortex

The earliest developmental stage of the central nervous system begins with the neural plate configuration of the neuroectoderm layer, which originates from the ectoderm and then results in the staggered folding of this structure to the final form called the neural tube. The neuroectoderm develops into the neuroepithelium, a polarized layer of cells that lines the inner side of the neural tube and consists of neuroepithelial stem cells (NESCs). Within this structure, there is a highly heterogeneous population of dividing NESCs, collectively referred to as neural progenitor cells (NPCs) (6,7).

Neurogenesis is supported by various cell division mechanisms that operate together. Before the onset of neurogenesis, NPCs divide symmetrically, multiplying their number and becoming the founder population of neurogenic ventricular radial glia (vRG) cells, which have cell bodies in the ventricular zone (VZ) (8). In mid-neurogenic stages, vRG cells divide asymmetrically to form one neuron and one NPC, or NPCs undergo symmetrical terminal division, where a progenitor cell divides to create two neurons, consequently depleting the pool of proliferative cells (9,10). NPCs in the cortical VZ are usually believed to divide in all three of these ways.

Another subgroup of self-renewing progenitors that have similar characteristics to vRGs are outer/basal radial glia (oRG) cells (11,12). oRGs are generated during the middle to late neurogenic stages during normal mammalian brain development (13). Even if oRGs can divide asymmetrically to replicate themselves and retain neural stem cell potential like vRGs, they lack an apical process or apicobasal polarity and also instead take on a special morphology, molecular identity and dynamic cell behavior (11,12,14).

The main striking difference is that vRG cells perform the process of interkinetic nuclear migration (IKNM) by dynamically moving their nuclei between apical and basal regions during the cell cycle; oRG cells use the mitotic somal translocation (MST) mechanism by rapidly moving their cell bodies in the basal direction during mitosis (15). For vRG cells attempting to divide in a limited area, IKNM, a nuclear oscillation phenomenon on the VZ surface, facilitates easy and efficient use of the region (16,17). As a basis, IKNM consists of a slow migration of the nucleus in the basal direction in the G1 phase, its stay on the basal side in the S phase and its migration back towards the apical direction in the G2 phase and following undergoes mitosis on the apical side (18). Actomyosin plays a role in this migration along the apical-basal axis. Research on mutations in genes associated with human lissencephaly, including LIS1, has demonstrated that IKNM within the layered architecture of the brain is linked to the microtubule motor system and reliant on dynein during the G2 phase and kinesin during the G1 phase (19,20).

In contrast to the actomyosin dependence of IKNM, non-muscle myosin II (NMII) and Rho effector ROCK, which affect the RhoA-ROCK-NMII pathway are needed instead of microtubule motor in oRG cells MST (21). MST could be a potential target in NDDs associated with various cortical malformations, such as certain types of microcephaly, periventricular nodular heterotopia (PNH), cobblestone malformations, and lissencephaly, which are influenced by genes involved in the RhoA-ROCK-NMII signaling pathway (21,22).

Asymmetric division of both types of radial glial cells does not always involve the necessity of forming a neuron, they can generate an intermediate progenitor (IP) cell instead of a neuron (15). The IP cells, often referred to as basal progenitor (BP) cells, engage in terminal symmetric division in the later phases of neurogenesis, resulting in the formation of two neuronal daughter cells (23,24). It is found that asymmetric divisions primarily take place in the VZ, while symmetric neurogenic divisions occur predominantly in the subventricular zone (SVZ) (23).

A critical determinant influencing the fate outcome of progenitor divisions is the orientation of the cleavage plane relative to the apicobasal axis. The orientation of the cleavage plane during progenitor cell division serves as a crucial factor in determining whether divisions are symmetric or asymmetric. The mitotic spindle, aligned along the polarity axis, orchestrates the distribution of cell fate determinants between daughter cells. Vertical cleavage planes, which are parallel to the apicobasal axis, can promote either symmetric or asymmetric outcomes depending on the inheritance of apical membrane components and associated polarity complexes. In contrast, oblique or horizontal cleavage planes, deviating from the apicobasal axis, often lead to asymmetric divisions by generating one progenitor and one neuron or IP cell (18).

The vertical cleavage plane can bypass both the polarity complexes, such as the PAR complex (Par3/Par6/aPKC), and the apical plasma membrane, because the apical plasma membrane constitutes only 2–3% of the total plasma membrane. In addition, the cytocortical protein complex, functioning as a lateral belt (LGN–Gαi–NuMA), can also be differentially distributed to daughter cells during asymmetric division. Similarly, aberrant localization of the Numb protein either apically or basally, as well as the functionality of Minibrain/DYRK1A or other cell cycle regulators, may serve as potential drivers. These findings underscore how cleavage plane disorientation impairs the fidelity of asymmetric divisions.

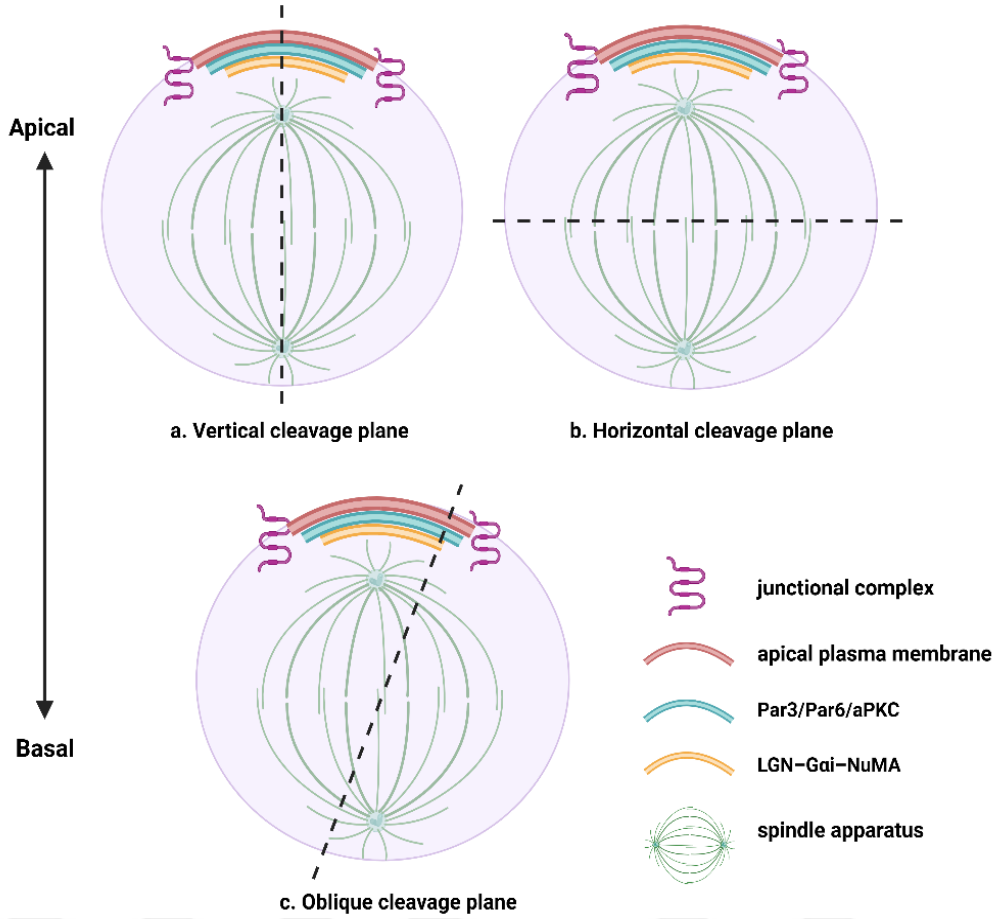

Figure 1. The possible orientations of the cleavage plane during cell division
Created in BioRender. Aral, M. (2025) https://BioRender.com/1v1j25r

2.1.2 Neuronal migration: guidance and regulation

Neuronal migration within the cerebral cortex initiates with the departure of the initial group of postmitotic neurons from the germinal VZ (25). In the process of corticogenesis, radial migration serves as the primary mechanism for neuronal movement, facilitating the translocation of one daughter nucleus to the cortical plate (CP) via the elongated, radially aligned basal process. It is pointed out that two distinct possible routes of radial migration: somal translocation and glia-guided migration (26).

In somal translocation seen in the early stages of cortical formation, the soma moves outward, while the cell body moves towards the pial surface through the retraction of its radial process, which remains fixed to the pial surface. Neurons that

employ glia-guided locomotion, by contrast, display a reduced radial process that does not extend to the pial surface, including the entire cell body moving cohesively, oriented along the radial glial fibers that serve as a structural scaffold (27).

It is clear that nucleokinesis, in other words, the movement of a nucleus, is a crucial part of radial migration. During nucleokinesis, both microtubules and their motor proteins work and organize together to shift the nucleus toward one end of the cell. The nuclear movement has been manipulated with several microtubule-dependent genetic processes such as the nuclear distribution (nud) mutants, to highlight the prominence of nucleokinesis (28,29). Current understanding suggests that the nuclear-distribution pathway is highly conserved across eukaryotic organisms and involves proteins that play crucial roles.

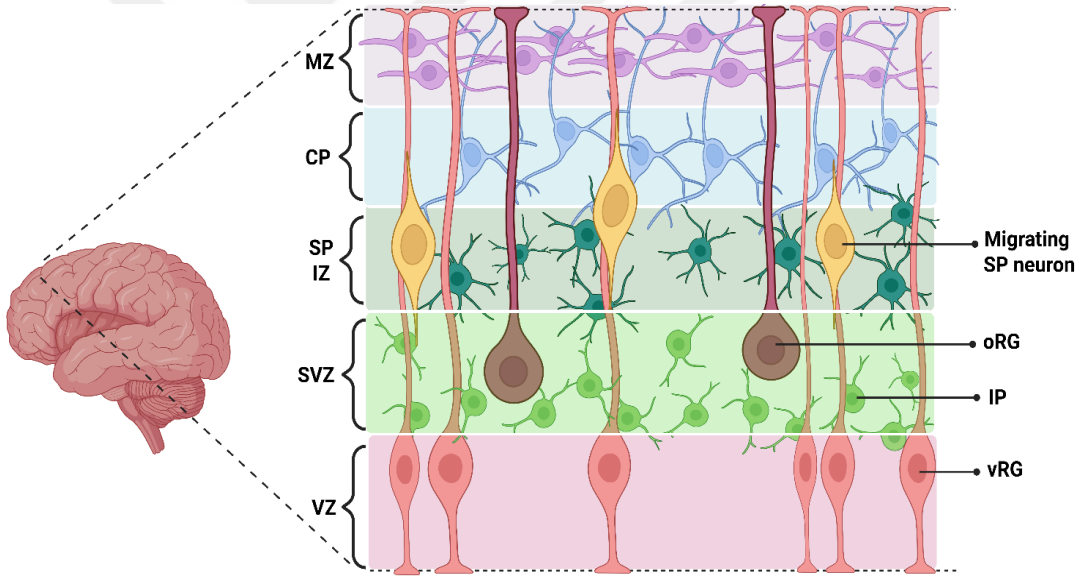

Figure 2. Positioning of the radial glial cells and newborn neurons across cortical zones
MZ, marginal zone; CP, cortical plate; SP, subplate; IZ, intermediate zone; SVZ, subventricular zone; VZ, ventricular zone. Created in BioRender. Aral, M. (2025) https://BioRender.com/qkm1izf

2.2 Cortical Malformations in Neurodevelopmental Disorders

MCDs are classified into three categories based on the stage at which the disruption in cortical development occurs. These structural brain abnormalities are characterized by defects in proliferation/apoptosis, neuronal migration, or late

migration/cortical organization (30). Disruptions occurring during the proliferation and apoptosis phase primarily influence brain size and cellular composition, leading to conditions such as megalencephaly, microcephaly, and focal cortical dysplasia (FCD). While megalencephaly and microcephaly result from alterations in neuronal number, FCD is also associated with structural abnormalities in neuronal morphology and organization.

Overproliferation of neuronal progenitor cells directly affects brain size by increasing the number of postmitotic neurons. This imbalance, whether driven by excessive proliferation or reduced apoptosis, leads to disorders like megalencephaly (31). Conversely, insufficient proliferation or increased apoptosis results in primary microcephaly, a condition marked by significantly reduced brain size, defined by a head circumference more than three standard deviations below the mean for age and sex (32,33). Additionally, abnormal proliferation can also lead to the formation of dysmorphic neurons, a hallmark of type II FCD. Specifically, FCD type IIa is characterized by dysmorphic neurons, while FCD type IIb is distinguished by the presence of both dysmorphic neurons and balloon cells, which are large, aberrant cells lacking specific glial or neuronal differentiation (34).

During subsequent stages of cortical development, errors in neuronal migration result in distinct cortical malformations, each associated with specific disruptions in neuronal positioning and connectivity. Notable disorders resulting from neuronal migration defects include heterotopia, lissencephaly and cobblestone malformations (35). Disruptions in the radial glial scaffold can lead to significant non-cell-autonomous defects in neuronal migration, resulting in PNH (30,36). In contrast, cell-autonomous neuronal migration disorders arise from intrinsic mechanisms and include conditions such as lissencephaly and subcortical band heterotopia (37), which represent opposite ends of the neuronal migration defect spectrum. Classic lissencephaly is characterized by a thickened cortex and a reduced number of gyri, ranging from a complete absence of gyri (agyria) to milder forms with broadened gyri (pachygyria). On the other hand, subcortical band heterotopia (also known as 'double cortex') is defined by bilateral bands of grey matter within the white matter, situated

between the lateral ventricles and the cerebral cortex (35,38). The failure of radial glial cells to properly adhere to the pial limiting membrane leads to excessive neuronal migration beyond the CP and into the leptomeninges, a characteristic of cobblestone malformations (also known as lissencephaly type II) (39,40).

Malformations arising from cortical organization defects involve disruptions in late neuronal migration and maturation, affecting normal cortical structure and function. Prominent examples within this category include polymicrogyria and schizencephaly (41,42). Among these, polymicrogyria is one of the most well-characterized disorders. Polymicrogyria is defined by the abnormal distribution of neurons after reaching the cortex, leading to the formation of multiple small gyri, which classifies it as a disorder of neuronal organization (43). Unlike lissencephaly, the cortex in polymicrogyria is not truly thickened but appears overfolded, sometimes giving the impression of increased thickness on imaging (44). Histologically, polymicrogyria exhibits a range of abnormalities, all involving disruption of the normal six-layered cortical architecture. While this alteration shares features with cortical dysplasia, polymicrogyria typically affects larger cortical regions rather than being restricted to focal disruptions containing dysplastic neurons (45,46).

Schizencephaly can arise from disturbances at any stage of cortical development—proliferation, migration, or organization. However, the presence of a polymicrogyric cortex adjacent to the cleft suggests that it is primarily a disorder of cortical organization (47,48). This neurological condition is characterized by full-thickness cerebral clefts extending through the affected hemisphere (49). Although these clefts can be multiple and may co-occur with contralateral polymicrogyria, schizencephaly remains a rarer entity compared to polymicrogyria (50).

2.2.1 Rare disease genetics: from genomic complexity to clinical phenotypes

Rare diseases are disorders that affect a small number of people compared to the general population. These conditions often elude common clinical and laboratory assessments, with approximately 80% following a Mendelian inheritance pattern

(51,52). It is estimated that rare diseases affect fewer than one individual per 2,000 people in Europe (53).

The genetic basis of rare diseases is highly heterogeneous, leading to variability in clinical presentation among affected individuals and populations. This complexity presents a significant challenge in identifying precise pathogenic mechanisms (54). Even among individuals diagnosed with the same syndrome, distinct genetic mutations can underlie similar phenotypic features, illustrating the concept of genetic heterogeneity. Discovering the causative genes of these disorders, particularly those with unknown etiology, is therefore crucial. NDDs exemplify this complexity, as mutations in various genes contribute to a broad and variable spectrum of psychiatric and neurological symptoms. However, these manifestations often lack specificity, making it difficult to pinpoint a definitive genetic cause. Depending on the classification criteria, NDDs can encompass hundreds to thousands of Mendelian syndromes, each with a low prevalence (55).

Beyond genotypic complexity, phenotypic variability further complicates disease characterization. Even within families, individuals carrying the same pathogenic variant can exhibit strikingly different phenotypic outcomes (56,57). To unravel the full spectrum of phenotypic variability in rare diseases, comprehensive genomic analysis is essential. Advances in whole-exome (WES) and whole-genome sequencing (WGS) have provided valuable insights, yet significant challenges remain in linking specific genetic alterations to clinical outcomes.

2.3 Microlissencephaly

Microlissencephaly (MLIS) is a rare but severe cortical malformation characterized by a combination of congenital microcephaly and lissencephaly. It is associated with significant neurodevelopmental impairment, and its diagnosis relies on both clinical and neuroimaging criteria (58). Microcephaly is typically defined as a head circumference measuring three or more standard deviations (SD) below the

population mean, while individuals with a head circumference between two and three SD below the mean often exhibit normal neurodevelopmental outcomes (59,60,61).

The clinical presentation of MLIS is highly variable (62). Affected individuals commonly present with microcephaly, along with bitemporal narrowing, a receding forehead, a mildly prominent occiput, hypertelorism, a broad and well-defined nasal bridge, and severe postnatal growth failure. Neurologically, they often exhibit hypertonia, hyperreflexia, seizures, and profound intellectual disability (63).

MRI plays a crucial role in characterizing the cortical architecture of MLIS and differentiating it from other cortical malformations. Imaging findings typically reveal an hourglass-shaped brain configuration with regions of pachygyria and agyria, underdeveloped Sylvian and Rolandic fissures, and incomplete opercularization of the insular areas. Additionally, there is an irregular pattern in the spacing of gyri and sulci, moderate cortical thickening (5–10 mm), and white matter signal abnormalities. Associated findings may include lateral ventricle enlargement, mild corpus callosum hypoplasia, and a persistent cavum septum pellucidum (63,64).

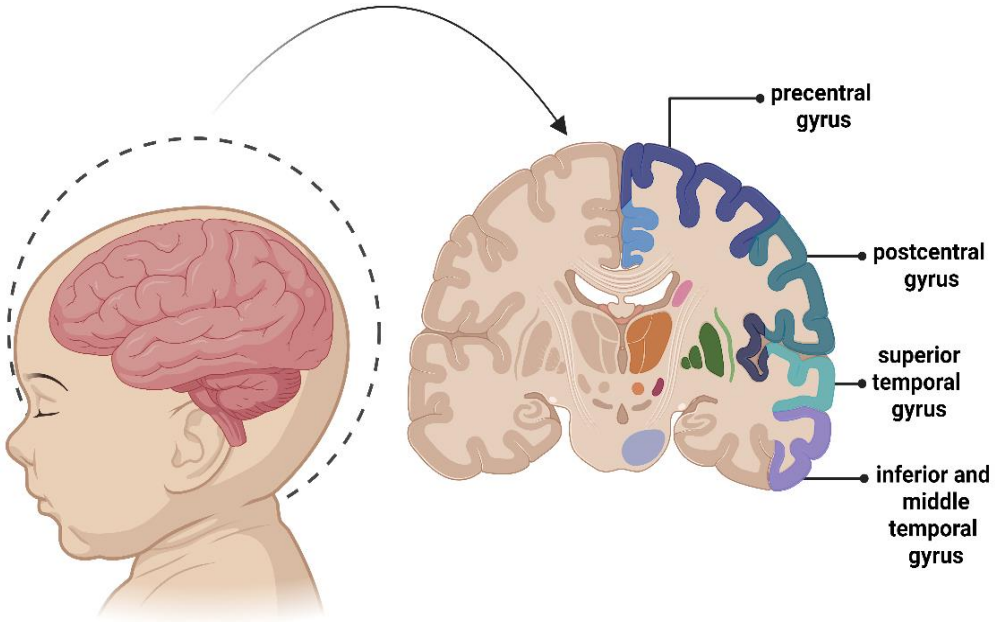

Figure 3. Microlissencephaly patient

Created in BioRender. Aral, M. (2025) https://BioRender.com/tx8578r

2.3.1 Congenital microcephalies and potential mechanisms

Congenital microcephaly can result from various prenatal factors, including viral infections, vascular ischemic-hemorrhagic injuries, exposure to alcohol or drugs, and genetic mutations. Genetic mutations will become prominent when investigating genetic causes. Genetically driven congenital microcephaly can be broadly categorized into two groups: microcephaly primary hereditary (MCPH), where microcephaly is the defining clinical feature, and microcephalic primordial dwarfisms (MPDs), such as Seckel syndrome, microcephalic osteodysplastic primordial dwarfism type II (MOPD II), and Meier-Gorlin syndrome (MGS), which involve microcephaly alongside generalized growth restriction (65).

Since the identification of the first MCPH-associated gene in 1998, a total of 25 genetic loci have been mapped as causative for primary hereditary microcephaly (66,67). In the case of Seckel syndrome, 10 genetic loci (corresponding to 9 genes) have been identified thus far. Notably, some genes implicated in Seckel syndrome have also been found in MCPH cases, indicating that these conditions exist along a phenotypic spectrum, differing primarily in the degree of short stature relative to microcephaly (67). MOPD II is characterized by skeletal anomalies, respiratory complications, microdontia, and intellectual disability, in addition to microcephaly and overall growth failure. Mutations in genes such as PCNT, IGF1RII, and NIN have been associated with MOPD II (68). Similarly, MGS is classified as a form of primordial dwarfism with distinct features, including microcephaly. Several components of the origin recognition complex (ORC) have been implicated in MGS, suggesting that disruptions or delays in DNA replication play a key role in its pathogenesis (65).

Table 1. Microcephalin genes (66,67)

Locus	Gene	Protein	Subcellular Location	Function/Pathway
MCPH1	*MCPH1*	Microcephalin 1	Nucleus and centrosome	DNA damage response, cell cycle checkpoint (G2-M) and chromosomal condensation
MCPH2	*WDR62*	WD-repeat-containing 62	Centrosome (interphase) and spindle poles (mitosis), Golgi-apparatus	Centriole biogenesis, mitotic spindle pole formation, scaffold for JNK pathway
MCPH3	*CDK5RAP2*	Cyclin-dependent kinase 5 regulatory subunit-associated protein 2	Centrosome	Centriole biogenesis, spindle and microtubule organization
MCPH4	*CASC5*	Kinetochore scaffold 1 (KNL1)	Kinetochore	Kinetochore integrity and spindle checkpoint activation in mitosis
MCPH5	*ASPM*	Abnormal spindle-like, microcephaly-associated protein	Centrosome and spindle pole during mitosis	Centriole biogenesis, spindle organization and kinetochore association
MCPH6	*CENPJ/CPAP /SAS-4*	Centromeric protein J	Centrosome (interphase)	Centriole biogenesis, spindle organization, cilia formation and kinetochore association
MCPH7	*STIL*	SCL/TAL1-interacting locus protein	Centrosome	Centriole biogenesis, ciliogenesis, cell cycle progression
MCPH8	*CEP135*	Centrosomal protein 135 kD	Centrosome	Centrosome organization, centriole duplication
MCPH9	*CEP152*	Centrosomal protein 152 kD	Centrosome	Centriole biogenesis and cell polarity/motility
MCPH10	*ZNF335*	Zinc finger protein 335	Nucleus	Transcriptional control of progenitor proliferation, neurogenesis and neuronal migration
MCPH11	*PHC1*	Polyhomeotic-like 1 protein	Nucleus	Cell cycle regulation and DNA damage response control
MCPH12	*CDK6*	Cyclin-dependent kinase 6	Centrosome	Cell cycle regulation, microtubule and spindle organization, and kinetochore association

Table 1. Microcephalin genes (66,67) (continued)

Locus	Gene	Protein	Subcellular Location	Function/Pathway
MCPH13	*CENPE*	Centromeric protein E	Kinetochore/centrosome	Microtubule/spindle organization and kinetochore association
MCPH14	*SASS6*	SAS-6 centriolar assembly protein	Centrosome	Centriole assembly through procentriole complex
MCPH15	*MFSD2A*	Major facilitator superfamily domain-containing protein 2A	Plasma membrane	Transport across blood-brain barrier
MCPH16	*ANKLE2*	Ankyrin repeat- and LEM domain-containing protein 2	Not well characterized	Proliferation of neuroprogenitor cells
MCPH17	*CIT*	Citron rho-interacting serine/threonine kinase	Midbody	Cytokinesis
MCPH18	*WDFY3/ALFY*	WD repeat and FYVE domain-containing 3/autophagy-linked FYVE	Nucleus and cytoplasm	Autophagy
MCPH19	*COPB2*	Coatomer protein complex subunit beta 2	Golgi	Golgi budding and vesicular trafficking
MCPH20	*KIF14*	Kinesin family protein 14	Midbody	Cytokinesis
MCPH21	*NCAPD2*	non-SMC condensin I complex subunit D2	Cytoplasm to nucleus (metaphase)	Chromosome condensation
MCPH22	*NCAPD3*	non-SMC condensin II complex subunit D3	Nucleus	Chromosome condensation
MCPH23	*NCAPH*	non-SMC condensin I complex subunit H	Cytoplasm to nucleus (metaphase)	Chromosome condensation
MCPH24	*NUP37*	Nucleoporin 37	Nuclear envelope	Nuclear pore/chromatin organization
MCPH25	*MAP11*	Microtubule associated protein 11	Mitotic spindles and midbody	Spindle dynamics and cytokinesis

Table 2. Seckel syndrome genes (67)

Seckel syndrome (SCKL)	Gene	Protein	Pathway
SCKL1	*ATR*	Ataxia telangiectasia and rad3-related	DNA damage response
SCKL2	*RBBP8/CTIP*	Retinoblastoma-binding protein 8/CTBP-interacting protein (CtIP)	DNA damage response
SCKL3	Not identified	Not identified	Not identified
SCKL4	*CENPJ/CPAP/SAS-4*	Centromeric protein J	Centriole biogenesis
SCKL5	*CEP152*	Centrosomal protein 152 kD	Centriole biogenesis
SCKL6	*CEP63*	Centrosomal protein 63 kD	Centriole biogenesis
SCKL7	*NIN*	Ninein	Centriole subdistal appendage protein required to anchor microtubules
SCKL8	*DNA2*	DNA replication helicase 2	DNA damage response
SCKL9	*TRAIP*	TRAF interacting protein	DNA damage response
SCKL10	*NSMCE2*	SMC5-SMC6 complex SUMO ligase	DNA damage response

2.3.1.1 Centrosomal defects in microcephaly

Centrosomes are essential for multiple cellular functions, including mitotic spindle formation, cell polarity, and DNA damage response. They also serve as basal bodies for cilia formation. Given their key role in neurogenesis, mutations in centrosome-related genes frequently result in microcephaly (69).

Defects in mitotic spindle orientation are implicated in centrosomal protein-related microcephaly by disrupting progenitor cell division symmetry, affecting neurogenesis and brain size (18). Mutations in centrosomal genes like CDK5RAP2 and NDE1 support this link, as their dysfunction leads to spindle orientation defects in both humans and animal models (70-75). CDK5RAP2 regulates the microtubule-organizing center, while NDE1 interacts with centrosomal components to control dynein function (76). Mouse models of these mutations exhibit spindle orientation defects, early cell cycle exit, neuron loss, and increased cell death, ultimately leading to microcephaly (77,78).

Beyond spindle orientation defects, centrosomal protein mutations can disrupt centrosome duplication, cause fragmentation, and lead to premature centriolar separation (65). These defects result in abnormal microtubule nucleation, multipolar spindle formation, chromosome missegregation, prolonged mitosis, cell cycle arrest, and apoptosis. STIL, essential for centriole duplication, is linked to MCPH7, with mutations causing either centrosome loss or amplification (79,80). Its overexpression also leads to excess centrosomes, disrupting spindle assembly and genomic stability, emphasizing centrosome duplication defects as a potential cause of microcephaly (80). Mutations in CENPJ, linked to MCPH6 and Seckel syndrome (SCKL4), cause centriole defects that disrupt spindle assembly, leading to microcephaly. CENPJ is essential for centriole biogenesis, and its loss in mice results in spindle pole defects, delayed mitosis, and activation of the p53-dependent cell death pathway, causing embryonic lethality around E8.5 (81).

Mutations in ASPM (MCPH5) are the most common cause of primary microcephaly, accounting for 25–50% of cases (82). ASPM, localized to spindle poles and centrosomes, was initially linked to spindle orientation defects, as knockdown studies in human cells and mice showed such abnormalities (75,83). However, some studies challenge this hypothesis, as ASPM mutant mice with truncated proteins exhibited microcephaly without cleavage plane defects, suggesting alternative mechanisms (84). Instead, an alternative mechanism suggests ASPM regulates neural progenitor division by controlling cyclin activity through ubiquitination, phosphorylation, and nuclear localization, influencing cell cycle progression and stem cell maintenance (85).

WDR62, the second most frequently mutated gene in primary microcephaly (MCPH2), is linked to a spectrum of cortical abnormalities, including simplified gyrification, pachygyria, corpus callosum agenesis or malformations, and cortical thickening (86,87,88). In mouse models, WDR62 depletion via in utero electroporation resulted in reduced neural stem cell proliferation, premature cell cycle exit, and early differentiation into IP, without a significant increase in mitotic activity or apoptosis (89,90). One proposed mechanism involves centrosome inheritance, as

WDR62 mutant mice exhibit abnormal centrosome segregation, correlating with impaired neural proliferation and reduced brain size (91). Overall, centrosomal integrity is fundamental for proper neurogenesis. Disruptions in spindle orientation, centrosome duplication, or asymmetric division collectively contribute to microcephaly, highlighting centrosome-related defects as a key pathogenic mechanism.

2.3.1.2 Genomic instability in microcephaly

Genomic instability is another pathway linked to microcephaly, arising from defective DNA repair or excessive cellular stress that overwhelms even high-fidelity repair mechanisms, leading to an increased mutation rate. This instability can occur during DNA replication, the DNA damage response and repair process, or chromosome assembly and segregation. The human neocortex is particularly sensitive to disruptions in genomic stability, as microcephaly is one of its most prevalent clinical manifestations (92).

Neural progenitors have an exceptionally short cell cycle compared to other cell types, requiring highly efficient DNA replication to support their rapid and time-limited expansion during neurogenesis. In MGS, mutations in several DNA replication complex components, including ORC1, ORC4, ORC6, CDT1, GMNN, and CDC45, have been identified (65). Specifically, ORC1 mutations in MGS are associated with defects in DNA origin licensing, replication initiation, G1-S transition, and S-phase progression (93). These findings indicate that impaired DNA replication, caused by mutations in key replication initiation factors, likely contributes to congenital microcephaly in ORC1-related MGS.

Neural progenitors exhibit heightened sensitivity to DNA damage, likely due to the replicative stress caused by their rapid proliferation. The DNA damage response is a complex network of cellular mechanisms that detect DNA damage, activate cell cycle checkpoints, initiate DNA repair pathways, and trigger apoptosis if the damage is severe and poses a significant risk (92). Three key PI3K-like protein kinases, ATM,

ATR, and PRKDC, play essential roles in this response (94). ATM and PRKDC respond to DNA double-strand breaks, while ATR detects DNA damage during S-phase, preventing mutations and genomic instability. Their functional interplay has been demonstrated in mouse models with single or combined mutations in ATM, ATR, or PRKDC, which exhibit varying cellular sensitivity to radiation exposure. In humans, PRKDC mutations have been linked to a rare genetic syndrome characterized by microcephaly, further highlighting its role in genome stability and neural development (92).

Various DNA repair pathways address different types of DNA damage, including base excision repair (BER), nucleotide excision repair (NER), homologous recombination repair (HRR), and non-homologous end joining (NHEJ) (92). BER and NER play key roles in repairing single-strand DNA breaks, while double-strand breaks (DSBs) represent the most severe form of DNA damage, potentially leading to apoptosis or mutagenesis. The BER pathway involves multiple cellular components, including APEX1 and PNKP, which work together to maintain genome integrity. Mutations affecting this pathway are associated with microcephaly, as seen in PNKP mutations, which lead to microcephaly accompanied by seizures (95). In terms of maintaining genome integrity, as well as DNA repair mechanisms, the correct progression of chromosome condensation and decatenation, which occurs throughout chromosome segregation, is crucial. The centromeric kinetochore, located on the centromere of a chromatid, serves as the binding site for spindle microtubules during cell division. It plays a crucial role in aligning chromatids at metaphase and ensuring the precise and timely segregation of sister chromatids. Recently, mutations in genes involved in centromeric kinetochore function have been linked to congenital microcephaly (96,97). CASC5 has been identified as the causative gene for MCPH4 in humans (98). Additionally, mutations in CENPE, which encodes CENP-E, a kinesin-like motor protein essential for spindle microtubule capture and kinetochore attachment during mitosis, result in MCPH13 and MPD (97). CENPE mutations lead to multiple mitotic abnormalities in affected individuals, resulting in defective chromosome segregation and cytokinesis failure. Compared to centrosome-associated spindle defects, kinetochore-related pathogenic mechanisms appear to be less

commonly implicated in microcephaly, indicating that additional defects in this pathway may still be uncovered.

2.3.1.3 Alternative mechanisms in microcephaly

Mutations in cytokinesis-related genes, such as CIT and KIF14, have been linked to congenital microcephaly (67). CIT encodes CIT-K, a key component of the midbody, an organelle that facilitates the final separation of dividing cells (99). CIT-K helps organize the midbody, influences mitotic spindle orientation, and interacts with ASPM (67,99). In humans, missense mutations in CIT cause primary microcephaly (MCPH17), while truncating mutations lead to MLIS (67). KIF14, a kinesin-3 family member, plays a crucial role in cytokinesis by interacting with CIT-K at the midbody (100). Recent studies have identified KIF14 mutations in multiple microcephaly-affected families.

In addition to defects in cytokinesis, disruptions in cell cycle regulation also contribute to microcephaly. However, cell cycle length is also a factor that affects neuron production during neurogenesis. A shorter cell cycle allows for faster neuron generation, while its progressive lengthening, particularly in the G1 phase, slows down neurogenesis over time. The G1-S transition is regulated by cyclin/CDK complexes, including CDK6, a key player in cell cycle progression (101). Mutations in CDK6 are linked to MCPH12, with patient fibroblasts displaying spindle disorganization, extra centrosomes, impaired motility, and reduced proliferation (102,103). Additionally, transcription factors that regulate cell cycle genes, such as ARX, have also been implicated in microcephaly (104). Remarkably, ARX mutations lead to abnormal brain development, including microcephaly, lissencephaly, and corpus callosum agenesis (105).

2.3.2 Lissencephaly

Lissencephaly refers to a group of neuronal migration disorders characterized by a smooth cerebral cortex due to defective neuronal migration of postmitotic neurons

from the VZ to the developing CP (106,107). This severe brain malformation presents with agyria, pachygyria, abnormal cortical layering, enlarged ventricles, and neuronal heterotopias. While lissencephaly is primarily classified into two main groups based on its etiology and associated malformations—classical lissencephaly and cobblestone lissencephaly—additional subtypes can also be considered, such as X-linked lissencephaly with agenesis of the corpus callosum (ACC), lissencephaly with cerebellar hypoplasia (LCH), and MLIS (63).

Several lissencephaly-related genes play a crucial role in microtubule function, essential for centrosome and nuclear movement in migrating neurons (108). Certain genes are specifically linked to cerebral cortex abnormalities. Mutations in six key genes—LIS1, DCX, TUBA1A, RELN, VLDLR, and ARX—have been associated with lissencephaly, while the co-deletion of YWHAE with LIS1 may act as a modifier (109). Additionally, mutations in tubulin isoforms contribute to a group of brain malformations known as tubulinopathies, which can present with different lissencephaly subtypes, PMG-like cortical dysplasia, a simplified gyral pattern, or MLIS.

Table 3. Lissencephaly genes (110)

Protein network	**Gene**
Tubulins	*TUBA1A*
	TUBB2B
	TUBA8
	TUBB
	TUBB3
Centrosome-expressed MAPs	*LIS1-YWHAE*
	LIS1
	TUBG1
	NDE1
Microtubule motor MAPs	*DYNC1H1*
	KIF5C
	KIF2A
Actin and actin-associated MAPs	*ACTB*
	ACTG1
	DCX

Table 3. Lissencephaly genes (110) (continued)

Protein network	Gene
Complex MAPs	*CDK5*
	Reelin signaling
	RELN
	VLDLR
Forebrain	*ARX*
Neuronal apoptosis	*CRADD*

2.3.2.1 Classical lissencephaly

Classical lissencephaly (type 1 lissencephaly) is a well-recognized neuronal migration disorder, characterized by a combination of agyria and pachygyria. This form of lissencephaly is associated with Miller-Dieker syndrome (MDS) and isolated lissencephaly sequence (ILS) (106). MDS is characterized by classic lissencephaly and distinct craniofacial abnormalities, such as a prominent forehead, bitemporal hollowing, a short upturned nose, a protuberant upper lip with a thin vermilion border, and micrognathia (111). In contrast, ILS is defined by classic lissencephaly in the absence of MDS-specific craniofacial features.

The LIS1 gene, located on chromosome 17p13.3, was the first gene linked to human lissencephaly (63,106,108). It encodes a microtubule-associated protein that primarily localizes to the centromere in migrating neurons and is highly conserved across species. LIS1 plays a crucial role in neuronal migration by regulating mitotic spindle orientation in NESCs and radial glial progenitors (63). It also helps maintain the microtubule network and interacts with multiple microtubule-associated proteins. LIS1 deletion disrupts dynein function, a key cytoplasmic motor protein essential for neuronal migration (63,108). Additionally, LIS1 regulates dynein activity, participating in intracellular transport, mitosis, and directed cell movement, where it works alongside dynein and dynactin at the leading edge of migrating cells.

ILS results from intragenic mutations or deletions of the LIS1 gene or small deletions affecting chromosome 17p13.3 (63,107,108). In contrast, MDS occurs when

both LIS1 and YWHAE are deleted, making it a contiguous gene deletion syndrome. The YWHAE gene, part of the 14-3-3 protein family, regulates phosphoproteins by preventing their dephosphorylation. It binds to CDK5/p35-phosphorylated NUDEL, a LIS1-binding protein, maintaining its phosphorylation (63). NUDEL and LIS1 work together to regulate cytoplasmic dynein heavy chain function, which is crucial for neuronal migration. Smaller deletions that remove only LIS1 (without YWHAE) lead to a milder form of lissencephaly. YWHAE is thought to act as a dosage-dependent modifier, influencing the severity of classical lissencephaly (112).

While LIS1 and YWHAE deletions are key contributors to classical lissencephaly, mutations in other microtubule-related genes, such as DCX, also should be considered. Mutations in the DCX gene on chromosome Xq22.3 are linked to classical lissencephaly in males and subcortical band heterotopia (SBH) in heterozygous females (63,106,108). A mother with SBH can pass a DCX mutation to her son, leading to lissencephaly, or to her daughter, resulting in SBH. DCX is expressed in postmitotic neurons, but not in proliferating VZ cells or mature neurons (63). It encodes a cytoplasmic protein that regulates neuronal migration by stabilizing microtubules. Most identified DCX mutations are missense or truncating mutations that disrupt its tubulin-binding domain, impairing microtubule function.

Tubulinopathies arise from pathogenic variants in six key genes (TUBA1A, TUBB2A, TUBB2B, TUBB3, TUBB5, and TUBG1) or biallelic mutations in TUBA8. Among these, TUBA1A mutations are strongly associated with the agyria-pachygyria-band spectrum of cortical malformations (108,113). TUBA1A encodes α-tubulin, a core component of microtubules, which are essential for neuronal migration and cortical development. Mutations in TUBA1A disrupt tubulin heterodimer folding and impair interactions with key microtubule-binding proteins, such as DCX and KIF1A. These defects compromise microtubule function, affecting the motility of neuronal progenitor cells, ultimately leading to cortical dysgenesis. The TUBA1A-related disorder exhibits a broad spectrum of cortical abnormalities, including microcephaly, agyria, and SBH (63,108). Intellectual disability is a hallmark feature, often accompanied by epilepsy and motor deficits. Given its autosomal dominant

inheritance, TUBA1A mutations are typically de novo, similar to LIS1 mutations in classical lissencephaly. Additionally, neuronal axonal guidance defects and early differentiation abnormalities likely contribute to its pathogenesis. While LIS1 and DCX mutations account for approximately 75% of ILS cases, TUBA1A mutations contribute to about 4% (108,113). Despite some phenotypic overlap, mutations in these three genes share common neurological features, including microcephaly, intellectual disability, epilepsy, and motor impairments, though their specific contributions to cortical malformations differ in severity and pattern.

In addition to these microtubule-related genes, other signaling pathways also contribute to lissencephaly. Among these, ARX and RELN play key roles in interneuron migration and cortical layering. The ARX gene plays a crucial role in neuronal precursor proliferation and forebrain differentiation and it is essential for the non-radial migration of interneurons from ventral regions to the developing cortex. While ARX mutations are a rare cause of lissencephaly, they can disrupt cortical development by impairing interneuron migration (109,114). Reelin (RELN) is a signaling glycoprotein secreted by Cajal-Retzius cells in the early cerebral cortex. It plays a pivotal role in neuronal migration, ensuring proper laminar organization of the cortex through activation of the reelin signaling pathway. Although RELN mutations are rare, affected individuals typically exhibit generalized pachygyria on neuroimaging (108,114). Also, the VLDLR gene encodes a receptor for RELN, functioning alongside APOER2 to transmit extracellular RELN signals into intracellular pathways that regulate neuronal positioning. VLDLR mutations lead to a phenotypically similar cortical malformation, albeit with milder gyral simplification (108). Together, these findings highlight how mutations in genes regulating microtubule function, neuronal migration, and cortical organization contribute to the diverse spectrum of classical lissencephaly.

2.3.2.2 Cobblestone lissencephaly

Cobblestone lissencephaly (type II lissencephaly) is characterized by aberrant neuronal overmigration beyond the pial surface, resulting in cortical layer

disorganization and a distinct cobblestone-like gyral pattern (63). It is frequently associated with congenital muscular dystrophies and ocular abnormalities and is a hallmark feature of Walker-Warburg syndrome (WWS), muscle-eye-brain disease (MEB), and Fukuyama congenital muscular dystrophy (FCMD) (107). Cobblestone lissencephaly follows an autosomal recessive inheritance pattern, with mutations in the POMT1, POMT2, FKTN, and FKRP genes contributing to its associated disorders (63).

Beyond these, X-linked lissencephaly with abnormal genitalia (XLAG) arises from pathogenic variants in the ARX gene and is clinically distinguished by postnatal-onset microcephaly and a lethal course in males during early infancy (115).

Lissencephaly with cerebellar hypoplasia is marked by profound cerebellar malformations, often coexisting with either classical or cobblestone lissencephaly, particularly affecting the hippocampus and brainstem (63).

Lastly, MLIS is distinct from other LIS1-associated variants due to the presence of severe microcephaly (63). However, its underlying genetic mechanisms remain only partially elucidated, highlighting a gap in current knowledge.

2.4 Sequencing Technologies

2.4.1 Sanger sequencing

In 1975, Sanger introduced the "plus and minus" method for DNA sequencing, marking a major transition toward modern sequencing techniques that have since dominated the field (116). A key advancement in this method was the use of polyacrylamide gels to separate DNA fragments synthesized by DNA polymerase based on their length (117).

Sanger's dideoxy sequencing, also known as sequencing by synthesis (SBS), involves a DNA-dependent polymerase generating a complementary strand from a

single-stranded DNA template. This process begins at the 3′ end, where deoxynucleotides (dNTPs) are incorporated in a sequence complementary to the template strand. Chain elongation occurs through phosphodiester bond formation between the 3′ hydroxyl of the growing strand and the 5′ phosphate of the incoming dNTP. The method relies on the ability of DNA polymerases to incorporate 2′,3′-dideoxynucleotide monophosphates (ddNMPs), which lack the necessary 3′ hydroxyl group for further elongation. As a result, when a ddNMP is incorporated, synthesis terminates at that position, generating DNA fragments of varying lengths. To determine the sequence, four separate reactions are set up, each containing the template, polymerase, all four dNTPs (one radioactively labeled), and a primer, along with a controlled ratio of one of the four ddNTPs (118). The resulting fragments are then separated via electrophoresis on a denaturing polyacrylamide gel, achieving single-nucleotide resolution. The banding pattern across four lanes, each corresponding to a specific nucleotide, allows direct readout of the sequence.

While highly effective, this manual approach was labor-intensive and time-consuming, leading to the development of automated sequencing methods in 1986. The introduction of automation significantly improved sequencing efficiency by integrating gel electrophoresis, fluorescent detection, and sequence analysis into a streamlined process (119). In early automated systems, sequencing reactions were manually loaded onto slab gels, while electrophoresis and band detection were automated. The sequence was determined by tracking the movement of fluorescently labeled DNA fragments past a detector. A major advancement in this transition was the replacement of radioactive labeling with fluorescent dyes, requiring the development of polymerases capable of incorporating these labels efficiently. This shift enabled automated base calling and enhanced both efficiency and safety.

Modern automated Sanger sequencing, classified as a first-generation sequencing technology, further refined this approach by replacing slab gels with capillary electrophoresis, allowing the simultaneous analysis of 8–96 sequencing reactions. In this system, either the primer or the chain-terminating ddNTPs are labeled with distinct fluorescent dyes (e.g., ddATP tagged with a green dye). As the fragments pass through

the detection region, they are excited by a laser, producing fluorescence emissions in four different colors (120). The sequence order is determined based on these emissions, enabling high-throughput base calling.

Raw fluorescence signals undergo multiple processing steps to ensure accuracy, including normalization of emission intensities, correction for dye mobility variations, and removal of signal cross-talk (121). Base-calling algorithms then assign nucleotide identities and evaluate sequence accuracy (122). A widely used quality metric, the Phred 20 (Q20) score, corresponds to a base call with an error probability of 1%, serving as the standard benchmark for high-quality sequencing data.

2.4.2 Next generation sequencing

Following the automated Sanger method, newer technologies have emerged under the name Next-Generation Sequencing (NGS). High-throughput NGS (HT-NGS) technologies have revolutionized human genome research by producing up to 100 times more data compared to the traditional Sanger-based capillary sequencers. Sequencing technologies comprise multiple methods that are generally classified into template preparation, sequencing methods, and imaging strategies.

2.4.2.1 Template preparation

There are two methods used for template preparation in sequencing technologies: clonally amplified templates originating from single DNA molecules and single DNA molecule templates.

2.4.2.1.1 Clonally amplified templates

In the amplified templates required imaging systems, the two most common methods are emulsion PCR (emPCR) and solid-phase amplification. Emulsion PCR (emPCR) is a method used to prepare sequencing templates in a cell-free system, providing a library of fragment or mate-pair targets is constructed, and adaptors

containing universal priming sites are ligated to the DNA ends (123). This allows complex genomes to be amplified using common PCR primers. Following ligation, the DNA is separated into single strands and captured onto beads under conditions that ensure one DNA molecule attaches to each bead. After successful amplification and enrichment, millions of emPCR beads can be immobilized on a polyacrylamide gel within a standard microscope slide, as in the Polonator; chemically crosslinked to an aminocoated glass surface, as used in the Life/APG and Polonator; or deposited into individual PicoTiterPlate wells, a method employed by Roche/454. Solid-phase amplification is an alternative approach for generating clonally amplified clusters that are randomly distributed across a glass slide from fragment or mate-pair templates (124). This technique involves two fundamental steps: the initial phase, where the single-stranded, single-molecule template undergoes priming and extension, followed by bridge amplification, a process in which the immobilized template hybridizes with nearby primers, creating densely packed clusters through repeated amplification cycles.

2.4.2.1.2 Single molecule templates

Instead of clonally amplified methods, particularly in terms of eliminating the need for PCR and requiring significantly less starting material for sequencing, single-molecule templates offer convenience. Before the NGS reaction, these single-molecule templates are typically immobilized onto solid supports through various techniques, including the covalent attachment of spatially distributed primer molecules, the direct covalent attachment of single-molecule templates, or the immobilization of spatially distributed single polymerase molecules (125).

There are key differences between sequencing clonally amplified and single-molecule templates. In clonal amplification, the resulting population consists of identical templates, each undergoing the sequencing reaction, and the observed signal represents a consensus of the nucleotides or probes incorporated across these identical templates during a given cycle. In contrast, single-molecule sequencing involves

templates that can each experience variable nucleotide or probe incorporations within the same cycle, making them more susceptible to variations in the sequence data.

2.4.2.2 Sequencing methods and imaging strategies

While the term sequencing by synthesis (SBS) broadly encompasses various DNA polymerase-dependent sequencing methods, these approaches can be more precisely categorized based on their underlying mechanisms. They are primarily classified into cyclic reversible termination (CRT), which relies on reversible terminators to regulate DNA synthesis; single-nucleotide addition (SNA), where nucleotides are incorporated individually in a controlled manner; and real-time sequencing, which enables continuous detection of nucleotide incorporation without termination. In addition to these polymerase-based strategies, sequencing by ligation (SBL) represents a distinct approach in which DNA ligase, rather than DNA polymerase, is responsible for nucleotide incorporation, offering an alternative mechanism for high-throughput sequencing (126).

2.4.2.2.1 Cyclic reversible termination

Cyclic reversible terminators (CRT) utilize a sequencing approach that relies on reversible terminators in a continuous cycle of nucleotide incorporation, fluorescence imaging, and cleavage. This method ensures controlled DNA synthesis, as DNA polymerase, bound to the primed template, incorporates only a single fluorescently labeled nucleotide complementary to the template strand. The key feature of CRT is its ability to terminate DNA synthesis after each incorporation, preventing unwanted extension. Following this step, unincorporated nucleotides are removed through washing, and fluorescence imaging is performed to identify the incorporated base. The process is then reset by cleaving both the fluorescent dye and the blocking group, allowing DNA synthesis to resume in the next cycle (127).

At the core of this method lies the reversible terminator, which exists in two forms: 3′ blocked and 3′ unblocked. Inspired by Sanger sequencing, where

dideoxynucleotides serve as chain terminators, the development of reversible blocking groups at the 3′ end of nucleotides allowed for precise control over synthesis, enabling efficient sequencing with cyclic termination and restoration. This approach has been widely adopted in next-generation sequencing platforms. The Illumina/Solexa Genome Analyzer integrates the four-color CRT method with clonally amplified templates, utilizing solid-phase amplification to generate sequencing clusters.

In contrast, Lasergene, Inc. was the first research group to demonstrate that attaching a small terminating group to the base of a 3′-unblocked nucleotide can function as an effective reversible terminator, leading to the development of Lightning Terminators (128). Building on this concept, Helicos BioSciences later introduced Virtual Terminators, which incorporate a second nucleoside analogue that acts as an inhibitor. A key challenge with these 3′-unblocked terminators is designing modifications that precisely halt DNA synthesis after a single base addition, as the unblocked 3′-OH group naturally facilitates further nucleotide incorporation. In addition to this innovation, Helicos BioSciences pioneered single-molecule sequencing with the HeliScope, a technology that eliminates the need for amplification by directly sequencing individual DNA molecules (129,130).

The key distinction between these platforms lies in their imaging strategies: Illumina employs a four-color system where each nucleotide is labeled with a distinct dye, facilitating highly accurate base calling from amplified clusters, whereas Helicos relies on Virtual Terminators, using a single fluorescent dye applied sequentially in a predetermined order, mimicking a single-nucleotide addition process. This results in one-color imaging, where the sequencing data reflects individual single-molecule templates rather than clonally amplified clusters.

2.4.2.2.2 Pyrosequencing

Pyrosequencing is a based on single-nucleotide addition, non-electrophoretic sequencing method that leverages bioluminescence to track DNA synthesis by detecting the release of inorganic pyrophosphate, which is enzymatically converted

into a measurable light signal (131). Unlike methods that rely on modified nucleotides to terminate synthesis, pyrosequencing controls DNA polymerase activity by introducing a single type of dNTP in limiting amounts. As the polymerase incorporates a complementary base, the primer is extended, and synthesis temporarily halts until the next nucleotide is supplied. The sequential addition of nucleotides generates distinct light signals, recorded as flowgrams, where the intensity and order of the peaks directly correspond to the underlying DNA sequence. First introduced in 2005 by 454 Life Sciences, the GS 20 became the pioneering NGS platform on the market, utilizing a combination of single-molecule emulsion PCR and pyrosequencing. Following its acquisition of 454 Life Sciences, Roche further refined the technology by launching the GS FLX titanium, an upgraded version of the instrument. Both systems operate on the same core principle, employing a PicoTiterPlate (PTP) as the flow cell, constructed from a fused fiber-optic bundle (132). In this system, DNA templates prepared via emPCR are loaded onto 1–2 million beads, which are then deposited into PTP wells. The titanium-coated PTP design significantly enhances read length and data accuracy by minimizing signal interference between adjacent wells containing clonally amplified template beads. Additionally, smaller beads carrying sulphurylase and luciferase are positioned around the template beads to facilitate bioluminescence. Nucleotides are sequentially introduced across the wells in a predefined order, and the emitted light signals are captured using a charge-coupled device (CCD) camera, enabling precise sequence determination.

2.4.2.2.3 Real-time sequencing

Real-time sequencing has emerged as the next major advancement in the commercial sector, with Pacific Biosciences at the forefront of its development. Unlike reversible terminator-based approaches, this method does not interrupt DNA synthesis but instead enables continuous monitoring of nucleotide incorporation. In essence, real-time sequencing captures the integration of dye-labeled nucleotides in real-time as DNA synthesis progresses. Pacific Biosciences' platform achieves this by anchoring individual DNA polymerase molecules to the base of zero-mode waveguide detectors,

allowing for direct sequencing as phospholinked nucleotides are incorporated into the elongating primer strand (133).

2.4.2.2.4 Sequencing by ligation

Sequencing by ligation (SBL) is a cyclic technique that, unlike CRT, relies on DNA ligase and utilizes either one-base-encoded or two-base-encoded probes. In this process, a fluorescently labeled probe hybridizes to its complementary sequence adjacent to the primed template, after which DNA ligase facilitates the attachment of the probe to the primer. Any unligated probes are then washed away, and fluorescence imaging is performed to identify the incorporated probe. The cycle is repeated either by employing cleavable probes that remove the fluorescent dye and restore a 5′-phosphate group for subsequent ligation or by replacing the primer to initiate a new hybridization step. Life/APG has commercialized this approach through its SBL-based platform, known as Support Oligonucleotide Ligation Detection (SOLiD) (134).

2.4.3 Bridging sequencing technologies and human genetic disorders

NGS platforms are valuable for various applications in human genome research, including whole-genome sequencing, whole-exome sequencing, de novo assembly, and more targeted sequencing. Additionally, they are essential for cataloging transcriptomes across cells, tissues, and organisms (RNA-seq), detecting single nucleotide polymorphisms, identifying genome-wide structural variations, profiling epigenetic marks, performing ChIP-seq, and advancing personal genomics (135). Among these techniques, whole exome sequencing (WES) specifically targets the exons or protein-coding regions of the genome, whereas whole genome sequencing (WGS) examines the entire genome. WES has proven particularly valuable for gene discovery in patients with conditions such as brain malformations, congenital heart disease, and NDDs. By providing a comprehensive and unbiased analysis of all known disease-causing genes, WES has become an indispensable tool in human genome research (136).

3 MATERIALS AND METHODS

3.1 Materials

3.1.1 Ethical statement

This study, conducted within the scope of the project titled 'Genomic and Functional Research of Developmental and Degenerative Childhood Neurological Diseases', was approved by the Medical Research Ethics Committee of Acibadem Mehmet Ali Aydinlar University in its meeting numbered 2024/10, in accordance with medical ethics.

3.1.2 Patients

In this study, nine patients from our in-house Turkish sample cohort exhibiting clinical features of both microcephaly and lissencephaly were investigated.

Table 4. Phenotypic characteristics of the cohort.

Cases	Cohort ID	Gender	Clinical Manifestations
1	NG31-1	Male	Microcephaly, Lissencephaly
2	NG958-1	Male	Lissencephaly, Microcephaly, Intellectual Disability, Simian Line, First Motor Neuron
3	NG1225-1	Female	Microcephaly, Lissencephaly
4	NG1330-1	Male	Microcephaly, Lissencephaly
5	NG1521-1	Male	Microcephaly, Epilepsy, Intellectual Disability, Polymicrogyria, Spasticity, Temporal Occipital Pachygyria, Corpus Callosum Agenesis, Lissencephaly
6	NG1677-1	Female	Microcephaly, Corpus Callosum Agenesis, Lissencephaly, Cleft Palate
7	NG2021-2	Female	Microcephaly, Lissencephaly
8	NG2692-1	Female	Microcephaly, Lissencephaly
9	NG2939-1	Male	Microcephaly, Lissencephaly

3.1.3 Core laboratory equipment and genomic services

- KAPA Taq ReadyMix PCR Kit (Roche, Switzerland)
- T100 Thermal Cycler (Bio-Rad Laboratories, USA)
- PowerPac Basic Power Supply (Bio-Rad Laboratories, USA)
- Wide Mini-Sub Cell GT Systems (Bio-Rad Laboratories, USA)
- Applied Biosystems 3730xL DNA Analyzer (Thermo Fisher Scientific, USA)

3.2 Methods

3.2.1 Whole exome sequencing

Intact DNA was extracted from peripheral blood cells. Whole-exome capture was performed using the SeqCap EZ Exome v2 (Roche NimbleGen) for most samples, while the xGen Exome Hyb Panel v1 (IDT) was used exclusively for NG2021-2 and NG2939-1. Sequencing was conducted on a HiSeq 2500 (Illumina) for all samples, except for NG2021-2 and NG2939-1, which were sequenced on a NovaSeq 6000 (Illumina) at the Yale Center for Genome Analysis.

3.2.2 Bioinformatics processing of WES data

Raw sequencing data in FASTQ format were preprocessed for downstream analysis. As a preliminary quality control step, sequencing quality metrics, including per-base sequence quality, GC content, sequence duplication levels, and adapter contamination, were evaluated using FASTQC. Following quality assessment, sequence reads were aligned to the GRCh38 reference genome using BWA-MEM (v0.7.15), resulting in BAM files, which store compressed, indexed, and efficiently accessible alignment data (137). After read alignment, variant calling and post-alignment processing were conducted using the Genome Analysis Toolkit (GATK; Broad Institute, Cambridge, MA, USA), a widely used software package for sequence data analysis (138). Indel realignment was performed to minimize alignment artifacts caused by short insertions or deletions (indels), improving downstream variant calling

accuracy. Additionally, base quality score recalibration (BQSR) was applied to correct sequencing artifacts and enhance variant detection reliability. Post-alignment quality metrics, including coverage distribution, duplicate read percentage, mapping efficiency, and on-target capture efficiency, were assessed using the CollectHsMetrics tool from the Picard suite, integrated within the GATK toolkit. These metrics provided a comprehensive evaluation of the depth and quality of coverage across exome target regions.

Then, HaplotypeCaller (GATK) was used for variant calling, generating a VCF file containing identified single nucleotide polymorphisms (SNPs) and indels with associated quality metrics and annotations. Finally, SnpEff (v5.1), ANNOVAR, and Ensembl Variant Effect Predictor were used for variant annotation, integrating functional predictions, gene impact assessments, and clinical significance interpretations (139,140,141).

3.2.3 Variant filtering, classification and prioritization

Starting from annotated VCF files, variants were filtered and prioritized based on:

- mode of inheritance (X-linked, autosomal recessive or autosomal dominant) according to the genetic condition;
- functional consequence (retaining exonic and splicing variants while excluding UTR, intronic, and synonymous non-splicing variants);
- minor allele frequency in the general population ($\leq 5x10^{-3}$ for homozygous and $\leq 5x10^{-5}$ for heterozygous variants to retain rare variants);
- genotype calls (in all members within the quartet, min read depth ≥ 4 for homozygous and ≥ 8 for heterozygous; genotype quality score ≥ 20; Phred score ≥ 30);
- evolutionary conservation analysis with computational tools (GERP++, phyloP), which determine the degree of conservation of the affected genomic position across multiple species, indicating potential functional importance;

- pathogenicity predictions using bioinformatic tools (CADD, REVEL, SIFT, MutationTaster), which assess the potential effects of amino acid substitutions on protein stability, structural integrity, and function.

The inheritance pattern and clinical findings of the prioritized variants were evaluated using OMIM (Online Mendelian Inheritance in Man) in accordance with the proposed inheritance model (142). The following databases were employed to provide information about the minor allele frequency in the general population: gnomAD (v4.1.0), UK Biobank, 1000 Genomes Project, Kaviar, and Iranome (143-147).

Retained variants were classified in one of five classes (benign, likely benign, variant of uncertain significance, likely pathogenic, pathogenic) according to the American College of Medical Genetics and Genomics and the Association for Molecular Pathology (ACMG/AMP) variant interpretation guidelines (148). In this study, all variants identified as benign, likely benign, uncertain significance, likely pathogenic or pathogenic were taken into account.

3.2.4 Sanger sequencing

The genomic coordinates of the identified variants were retrieved using the University of California, Santa Cruz (UCSC) Genome Browser on the GRCh38 reference genome (149). Based on these coordinates, unique primers were designed using Primer3 (v4.1.0). Primer specificity was evaluated using UCSC In-Silico PCR to confirm target-specific amplification. To ensure optimal primer efficiency, key parameters such as melting temperature (Tm), GC content, and secondary structure formation were assessed using OligoAnalyzer (IDT) (150). PCR amplification was performed using the KAPA Taq ReadyMix PCR Kit (Roche, Switzerland) on a T100 Thermal Cycler (Bio-Rad Laboratories, USA). The success of amplification was verified by agarose gel electrophoresis using the Wide Mini-Sub Cell GT System and PowerPac Basic Power Supply (Bio-Rad Laboratories, USA). The resulting PCR products were purified and subsequently sequenced on an Applied Biosystems 3730xL DNA Analyzer (Thermo Fisher Scientific, USA) at the Yale University Keck Facility.

Sanger sequencing chromatograms were visualized and analyzed by SnapGene (v8.0.2).

3.2.5 Structural variation analysis

Copy number variation analysis was conducted using CNVkit (v0.9.12), a Python-based toolkit for targeted sequencing data (151). Control datasets were generated by selecting BAM files from individuals sequenced with the same capture kit as the test samples and who did not present with NDDs. A BED file was used to exclude off-target regions. Under these conditions, a minimum of three distinct control datasets were selected and matched to test samples based on gender (female/male). Due to the inherent coverage bias in capture-based sequencing, leading to non-uniform read depth, log2 ratio values were assessed, and the inferred copy number for each bin was visualized after rounding to facilitate interpretation.

In addition to detecting copy number changes, structural variant (SV) analysis was carried out directly from paired-end read alignments utilizing Manta (v1.6.0), a high-resolution algorithm designed to identify a wide range of germline SVs, including deletions, duplications, inversions, and translocations (152). The GRCh38 reference genome and the test BAM files were provided as inputs. Manta was executed in germline mode using default parameters, yielding three output VCF files: (i) unfiltered structural variants, (ii) unfiltered small indel candidates, and (iii) score-filtered variants based on a diploid genotyping model.

Score-filtered variants were evaluated to minimize false-positive calls. These outputs were subsequently annotated using AnnotSV (v3.4.2) to interpret the genomic coordinates of structural variants and their potential clinical relevance (153).

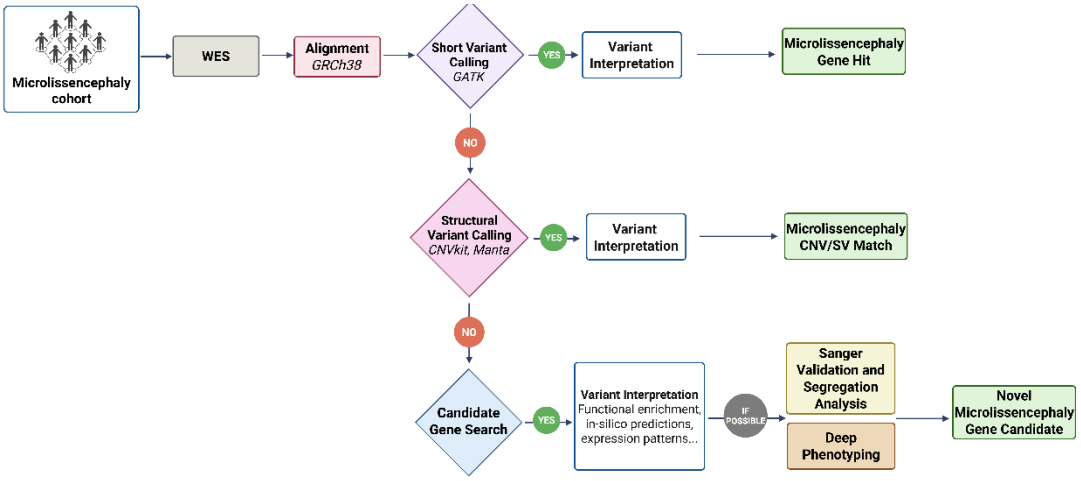

Figure 4. Decision tree flowchart

Created in BioRender. Aral, M. (2025) https://BioRender.com/zt5q8qq

3.2.6 Inbreeding coefficient analysis

PLINK (v1.9) software was utilized to evaluate the degree of autosomal homozygosity and estimate the inbreeding coefficient (F) (154). For each individual, both the observed and expected counts of homozygous genotypes were computed. The inbreeding coefficient (F) was then calculated using the method-of-moments approach, applying the following formula. Expected homozygosity values were derived based on minor allele frequencies (MAF) to ensure an unbiased assessment of deviations from Hardy-Weinberg equilibrium.

$$F = \frac{(observed\ homozygous\ count\ -\ expected\ homozygous\ count)}{(total\ genotypes\ -\ expected\ homozygous\ count)}$$

4 RESULTS

4.1 Pedigrees of the MLIS Patients

Pedigrees of the nine patients diagnosed with MLIS are presented below, based on familial information obtained from clinical records and structured family interviews. In several instances, information regarding the parents or extended relatives was incomplete or unavailable. These pedigrees were analyzed to assess inheritance patterns and to evaluate the segregation of candidate variants within each family.

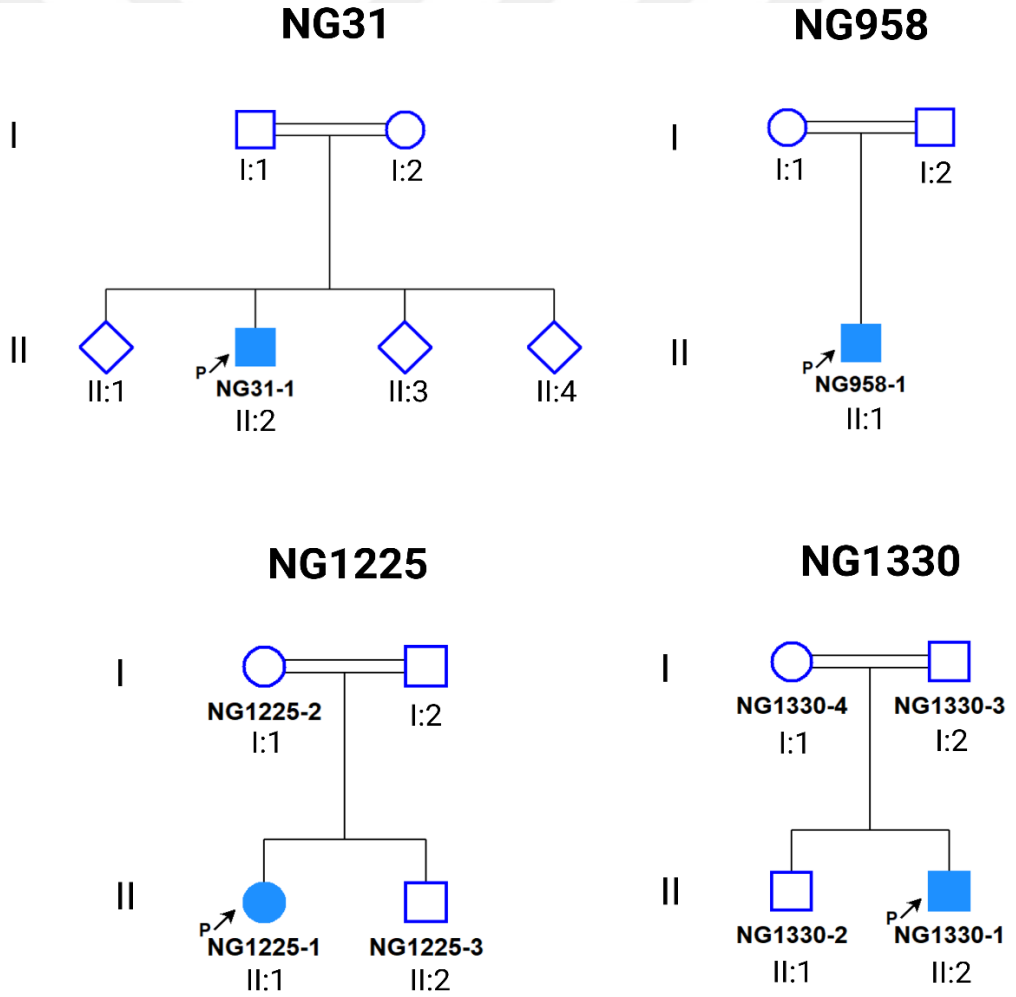

Figure 5. Pedigrees of patients with microlissencephaly

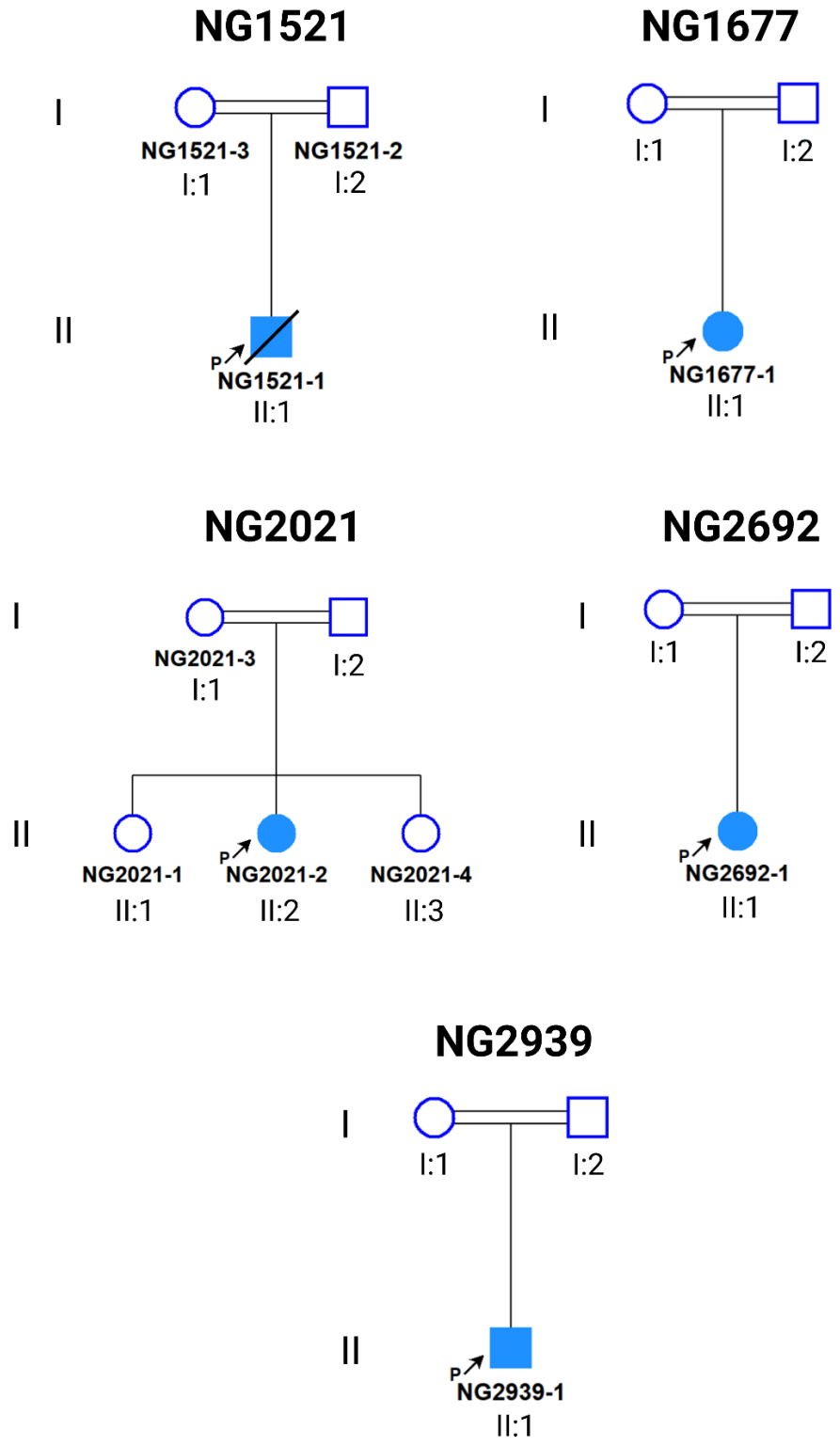

Figure 5. Pedigrees of patients with microlissencephaly (continued)

4.2 WES Data Quality Control Metrics

Key quality control (QC) metrics of WES data are listed as follows.

Table 5. QC metrics

	NG31-1	NG958-1	NG1225-1
Read length	74	76	76
Num of reads (M)	69.1	107.7	92.5
Num of bases (G)	5.1	8.2	7.0
Mean coverage	33.6	129.2	107.6
Median coverage	30	112	94
PCR duplicates	52.15%	7.88%	5.29%
Multiply mapped	2.97%	5.09%	5.63%
Unmapped	1.18%	2.80%	2.50%
Reads on-target	31.41%	72.59%	70.73%
Bases on-target	23.59%	56.66%	54.94%
Mean error rate	0.33%	0.71%	0.70%
1X target base coverage	95.9%	97.7%	97.7%
2X target base coverage	94.6%	97.2%	97.1%
4X target base coverage	92.2%	96.2%	96.2%
8X target base coverage	87.2%	94.7%	94.6%
10X target base coverage	84.4%	94.0%	93.8%
15X target base coverage	76.8%	92.3%	92.3%
20X target base coverage	68.6%	90.4%	89.8%
30X target base coverage	51.7%	86.7%	85.4%
40X target base coverage	36.1%	82.6%	80.4%
50X target base coverage	23.4%	78.3%	75.0%
100X target base coverage	0.8%	55.3%	46.8%
Targets	v2	v2	v2

Table 5. QC metrics (continued)

	NG1330-1	NG1521-1	NG1677-1
Read length	76	76	76
Num of reads (M)	75.5	91.4	116.5
Num of bases (G)	5.7	6.9	8.9
Mean coverage	87.9	110.1	119.4
Median coverage	77	92	104
PCR duplicates	6.35%	4.48%	2.99%
Multiply mapped	5.81%	5.70%	5.81%
Unmapped	0.90%	1.08%	0.23%
Reads on-target	70.95%	73.08%	64.02%
Bases on-target	54.93%	56.87%	48.41%
Mean error rate	0.33%	0.55%	0.46%
1X target base coverage	97.4%	97.5%	98.4%
2X target base coverage	96.8%	96.8%	98.0%
4X target base coverage	95.8%	95.7%	97.1%
8X target base coverage	94.0%	93.8%	95.7%
10X target base coverage	93.1%	92.8%	95.0%
15X target base coverage	90.8%	90.6%	93.4%
20X target base coverage	88.4%	88.2%	91.6%
30X target base coverage	82.7%	83.1%	87.6%
40X target base coverage	76.4%	77.8%	83.1%
50X target base coverage	69.5%	72.3%	78.2%
100X target base coverage	35.9%	46.7%	52.1%
Targets	v2	v2	v2

Table 5. QC metrics (continued)

	NG2021-2	NG2692-1	NG2939-1
Read length	101	76	101
Num of reads (M)	45.4	71.1	44.7
Num of bases (G)	4.6	5.4	4.5
Mean coverage	52.4	58.3	56.5
Median coverage	51	52	54
PCR duplicates	19.43%	6.06%	14.83%
Multiply mapped	5.85%	5.40%	5.66%
Unmapped	0.07%	0.11%	0.04%
Reads on-target	59.46%	53.62%	64.68%
Bases on-target	44.34%	38.74%	48.54%
Mean error rate	0.28%	0.33%	0.29%
1X target base coverage	98.2%	98.7%	99.0%
2X target base coverage	97.9%	98.4%	98.9%
4X target base coverage	97.5%	97.8%	98.8%
8X target base coverage	96.8%	96.3%	98.7%
10X target base coverage	96.4%	95.4%	98.6%
15X target base coverage	95.4%	92.3%	98.1%
20X target base coverage	93.7%	88.3%	96.8%
30X target base coverage	85.8%	77.5%	89.9%
40X target base coverage	71.4%	65.0%	76.7%
50X target base coverage	52.5%	52.5%	58.6%
100X target base coverage	2.8%	13.1%	4.3%
Targets	IDT	v2	IDT

4.3 Inbreeding Coefficient Scores

Inbreeding coefficient (IBC) scores were summarized in the following table, along with the corresponding estimated degrees of parental relatedness. (1C, first cousin; 1C1R, first cousin once removed; 1C2R, first cousin second removed)

Table 6. IBC scores

	NG31-1	**NG958-1**	**NG1225-1**
IBC **Parental Relation**	0.0408 ~1C1R	0.031 ~1C1R	0.028 ~1C1R
	NG1330-1	**NG1521-1**	**NG1677-1**
IBC **Parental Relation**	0.0533 ~1C	0.0331 ~1C1R	0.0394 ~1C1R
	NG2021-2	**NG2692-1**	**NG2939-1**
IBC **Parental Relation**	0.05 ~1C	0.0436 ~1C1R	0.0231 ~1C2R

4.4 Short Variant Findings

Identified variants in MLIS-related genes are summarized below for each patient.

Table 7. Annotated results of the prioritized variant in NG31-1

<table>
<tr><th colspan="4">NG31-1</th></tr>
<tr><th>Variant Information</th><th>Population Allele Frequency</th><th>Pathogenicity Scores</th><th>Evolutionary Conservation</th></tr>
<tr><td>Gene: PDCD6IP</td><td>gnomAD: 0</td><td>CADD: 34</td><td rowspan="3">GERP++: -</td></tr>
<tr><td>Genomic position:
GRCh38(chr3):g.33864130G>A</td><td>Iranome: 2</td><td>REVEL: -</td></tr>
<tr><td>Alteration at the transcript level:
NM_013374.6</td><td>UK biobank: 0</td><td>SIFT: -</td></tr>
<tr><td>Molecular consequence:
splice donor variant</td><td>1000G: 0</td><td>MutationTaster:
1,1</td><td rowspan="3">phyloP: 8.066</td></tr>
<tr><td rowspan="2">Zygosity: homozygous</td><td>Kaviar: 0</td><td rowspan="2">ACMG: Likely Pathogenic</td></tr>
<tr><td>In-house Turkish sample cohort: 2</td></tr>
</table>

Table 8. Annotated results of the prioritized variant in NG1225-1

<table>
<tr><th colspan="4">NG1225-1</th></tr>
<tr><th>Variant Information</th><th>Population Allele Frequency</th><th>Pathogenicity Scores</th><th>Evolutionary Conservation</th></tr>
<tr><td>Gene: ACTG1</td><td>gnomAD: 0</td><td>CADD: 28.4</td><td rowspan="3">GERP++: 4.05</td></tr>
<tr><td>Genomic position: GRCh38(chr17):g.81511046T>A</td><td>Iranome: 0</td><td>REVEL: 0.951</td></tr>
<tr><td>Alteration at the transcript level: NM_001614.5</td><td>UK biobank: 0</td><td>SIFT: 0.016</td></tr>
<tr><td>Molecular consequence: missense variant</td><td>1000G: 0</td><td>MutationTaster: 0.9999</td><td rowspan="3">phyloP: 7.622</td></tr>
<tr><td rowspan="2">Zygosity: heterozygous</td><td>Kaviar: 0</td><td rowspan="2">ACMG: Likely Pathogenic</td></tr>
<tr><td>In-house Turkish sample cohort: 1</td></tr>
</table>

Table 9. Annotated results of the prioritized variant in NG1330-1

<table>
<tr><th colspan="4">NG1330-1</th></tr>
<tr><th>Variant Information</th><th>Population Allele Frequency</th><th>Pathogenicity Scores</th><th>Evolutionary Conservation</th></tr>
<tr><td>Gene: DCX</td><td>gnomAD: 0.000501</td><td>CADD: 20.9</td><td rowspan="3">GERP++: 4.46</td></tr>
<tr><td>Genomic position: GRCh38(chrX):g.111330994C>A</td><td>Iranome: 0</td><td>REVEL: 0.02</td></tr>
<tr><td>Alteration at the transcript level: NM_001195553.2</td><td>UK biobank: 0.00045</td><td>SIFT: 0.442</td></tr>
<tr><td>Molecular consequence: missense variant</td><td>1000G: 0</td><td>MutationTaster: 0.5306</td><td rowspan="3">phyloP: 2.868</td></tr>
<tr><td rowspan="2">Zygosity: hemizygous</td><td>Kaviar: 0.00038</td><td rowspan="2">ACMG: Likely Benign</td></tr>
<tr><td>In-house Turkish sample cohort: 4</td></tr>
</table>

Table 10. Annotated results of the prioritized variant in NG1677-1

<table>
<tr><th colspan="4">NG1677-1</th></tr>
<tr><th>Variant Information</th><th>Population Allele Frequency</th><th>Pathogenicity Scores</th><th>Evolutionary Conservation</th></tr>
<tr><td>Gene: TUBA1A</td><td>gnomAD: 0</td><td>CADD: 24.4</td><td rowspan="3">GERP++: 5.51</td></tr>
<tr><td>Genomic position: GRCh38(chr12):g.49185206G>A</td><td>Iranome: 0</td><td>REVEL: 0.823</td></tr>
<tr><td>Alteration at the transcript level: NM_006009.4</td><td>UK biobank: 0</td><td>SIFT: 0.439</td></tr>
<tr><td>Molecular consequence: missense variant</td><td>1000G: 0</td><td>MutationTaster: 0.9999</td><td rowspan="3">phyloP: 9.365</td></tr>
<tr><td rowspan="2">Zygosity: heterozygous</td><td>Kaviar: 0</td><td rowspan="2">ACMG: Pathogenic</td></tr>
<tr><td>In-house Turkish sample cohort: 1</td></tr>
</table>

Table 11. Annotated results of the prioritized variant in NG2021-2

<table>
<tr><th colspan="4">NG2021-2</th></tr>
<tr><th>Variant Information</th><th>Population Allele Frequency</th><th>Pathogenicity Scores</th><th>Evolutionary Conservation</th></tr>
<tr><td>Gene: PPFIBP1</td><td>gnomAD: 0.0024</td><td>CADD: 16.04</td><td rowspan="3">GERP++: 0.191</td></tr>
<tr><td>Genomic position: GRCh38(chr12):g.27691891G>A</td><td>Iranome: 0</td><td>REVEL: 0.043</td></tr>
<tr><td>Alteration at the transcript level: NM_003622.4</td><td>UK biobank: 0</td><td>SIFT: 0.321</td></tr>
<tr><td>Molecular consequence: missense variant</td><td>1000G: 0.01817</td><td>MutationTaster: 0.6099</td><td rowspan="3">phyloP: 0.737</td></tr>
<tr><td rowspan="2">Zygosity: homozygous</td><td>Kaviar: 0.00672</td><td rowspan="2">ACMG: Benign</td></tr>
<tr><td>In-house Turkish sample cohort: 18</td></tr>
</table>

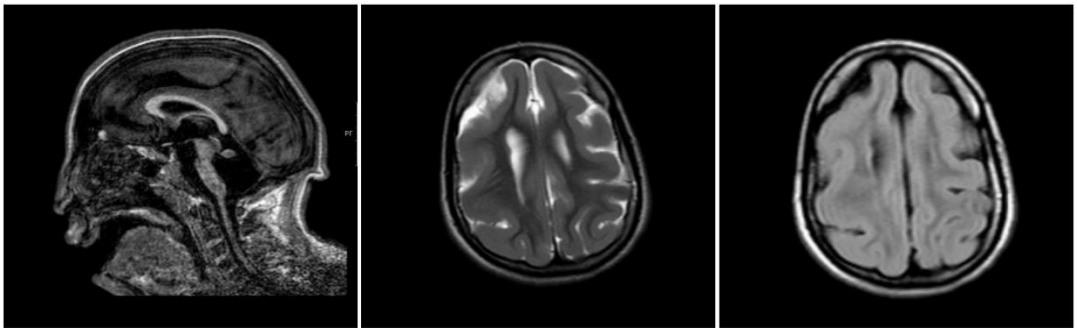

Figure 6. T1-weighted sagittal (left), T2-weighted axial (middle), and FLAIR axial (right) brain MRI images of patient NG2021-2

Table 12. Annotated results of the prioritized variant in NG2939-1

<table>
<tr><th colspan="4">NG2939-1</th></tr>
<tr><th>Variant Information</th><th>Population Allele Frequency</th><th>Pathogenicity Scores</th><th>Evolutionary Conservation</th></tr>
<tr><td>Gene: ACTB</td><td>gnomAD: 0</td><td>CADD: 27.9</td><td rowspan="3">GERP++: 5.55</td></tr>
<tr><td>Genomic position: GRCh38(chr7):g.5528086C>A</td><td>Iranome: 0</td><td>REVEL: 0.953</td></tr>
<tr><td>Alteration at the transcript level: NM_001101.5</td><td>UK biobank: 0</td><td>SIFT: 0.006</td></tr>
<tr><td>Molecular consequence: missense variant</td><td>1000G: 0</td><td>MutationTaster: 1</td><td rowspan="3">phyloP: 7.622</td></tr>
<tr><td rowspan="2">Zygosity: heterozygous</td><td>Kaviar: 0</td><td rowspan="2">ACMG: Likely Pathogenic</td></tr>
<tr><td>In-house Turkish sample cohort: 1</td></tr>
</table>

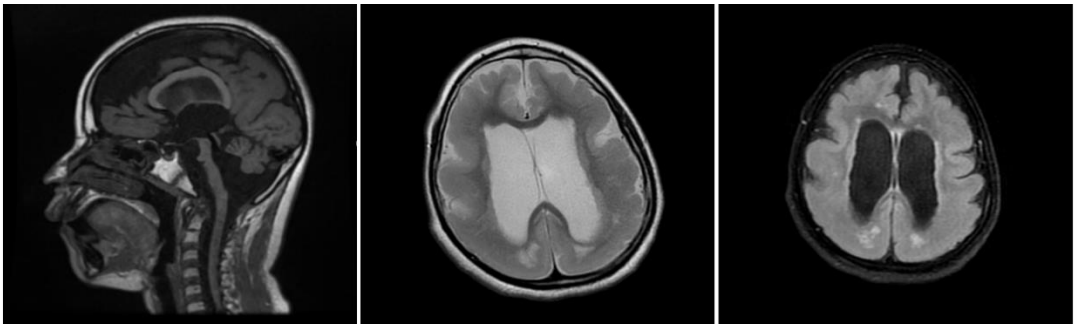

Figure 7. T1-weighted sagittal (left), T2-weighted axial (middle), and FLAIR axial (right) brain MRI images of patient NG2939-1

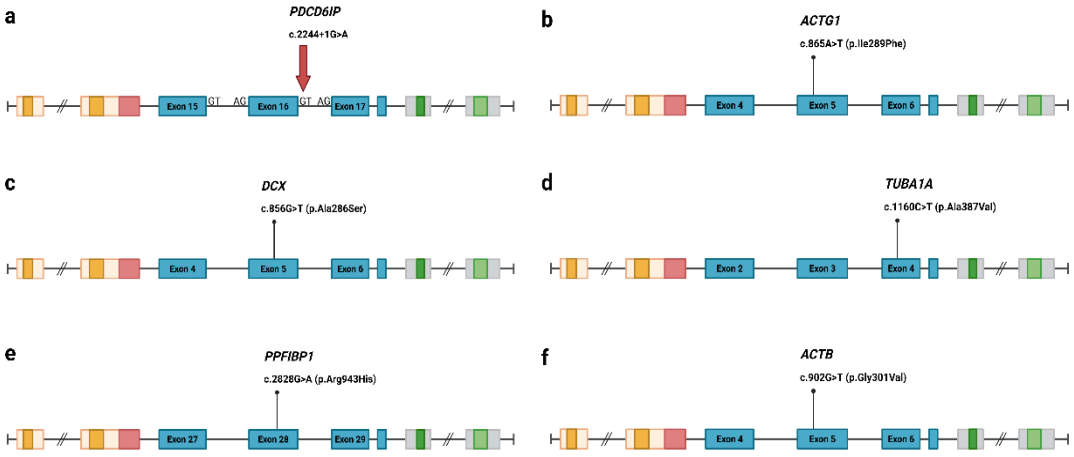

Figure 8. Schematic representation of the six prioritized variants mapped onto their respective gene structures (not to scale)

Created in BioRender. Aral, M. (2025) https://BioRender.com/bfmadia

Secondary homozygous variants identified in some patients, in addition to the primary variants, were evaluated according to variant filtering and prioritization criteria, and are presented in Table 13 based on their potential roles in disease-relevant genes.

Table 13. Secondary homozygous variants in disease-relevant genes.

Cohort ID	**Gene**	**Genomic position**	**Molecular consequence**	**In-house Turkish sample cohort allele count**
NG31-1	*BPTF*	GRCh38(chr17):g.67946029C>G	missense variant	10
NG1330-1	*CNTN4*	GRCh38(chr3):g.3026107A>G	missense variant	2
NG2021-2	*SMC4*	GRCh38(chr3):g.160431799G>T	missense variant	4
NG2692-1	*SLC25A24*	GRCh38(chr1):g.108192528C>T	missense variant	2

4.5 Detection of Copy Number and Structural Variants

Copy number profiles analyzed by CNVkit are shown below. Each diagram presents chromosome-specific results in two adjacent vertical tracks: the left segment highlights significant alterations (deletions or duplications), while the right track displays log2 coverage ratios for each targeted region in greater detail, shown as bins. White gaps indicate regions lacking targeted probes or insufficient coverage.

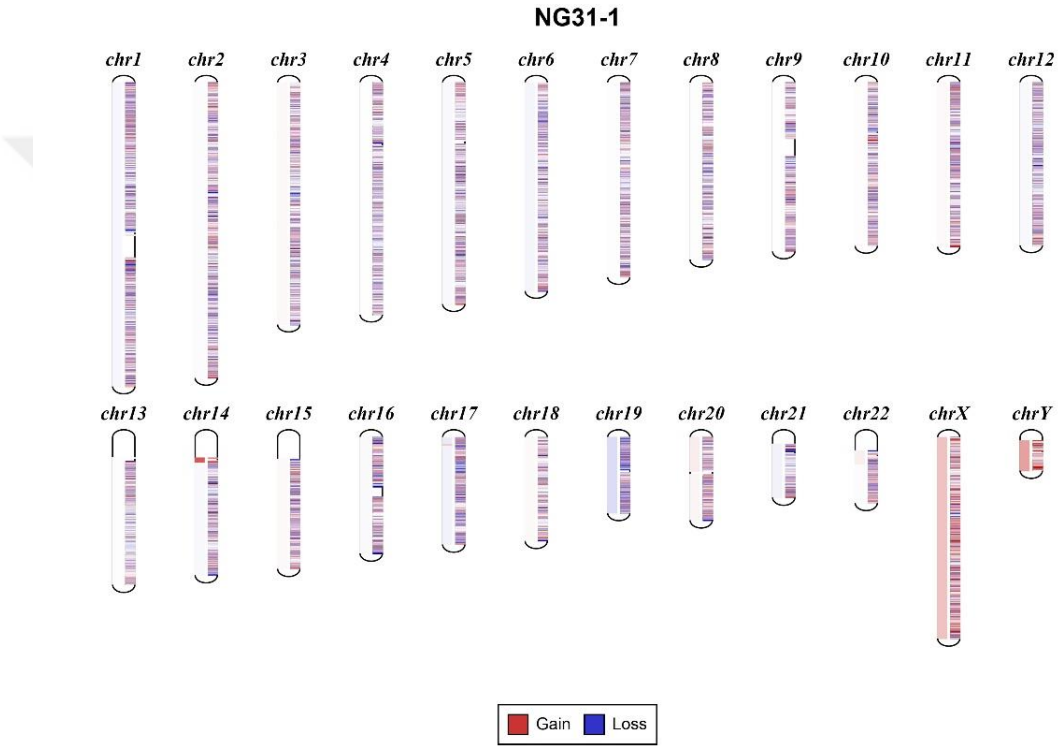

Figure 9. Genome-wide CNV profile of NG31-1

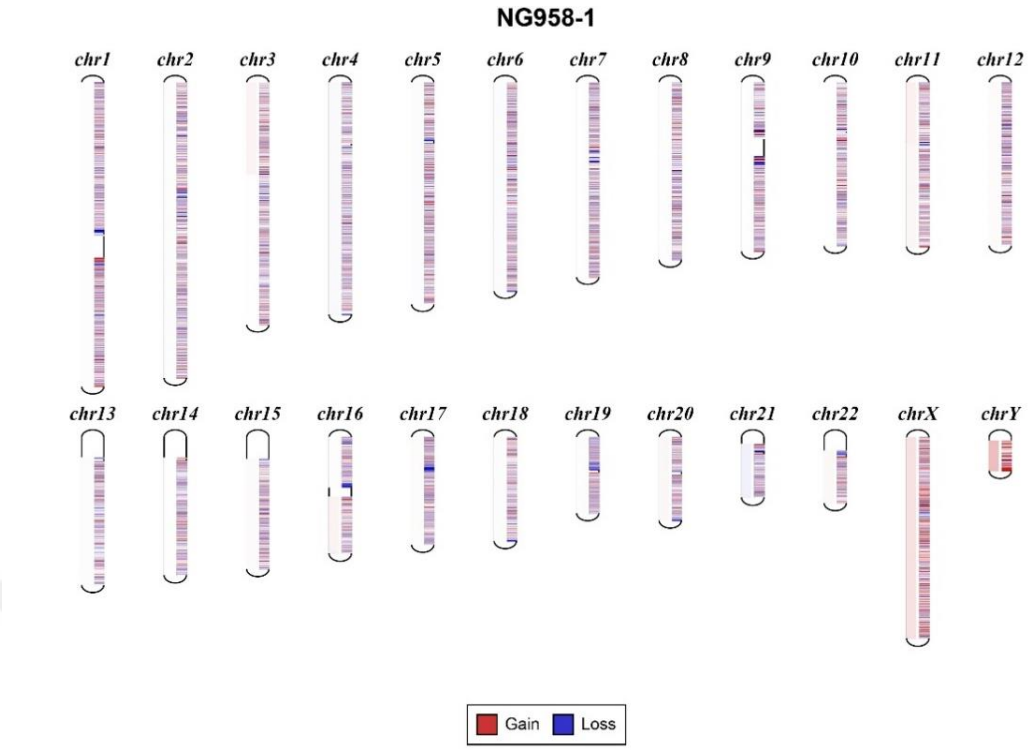

Figure 10. Genome-wide CNV profile of NG958-1

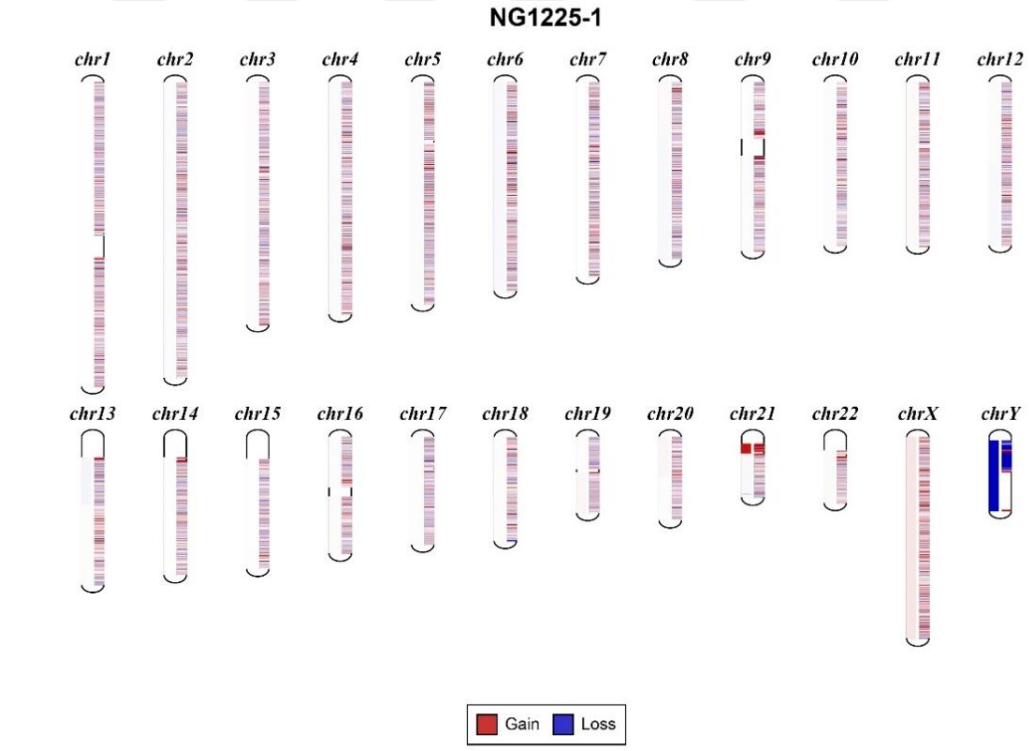

Figure 11. Genome-wide CNV profile of NG1225-1

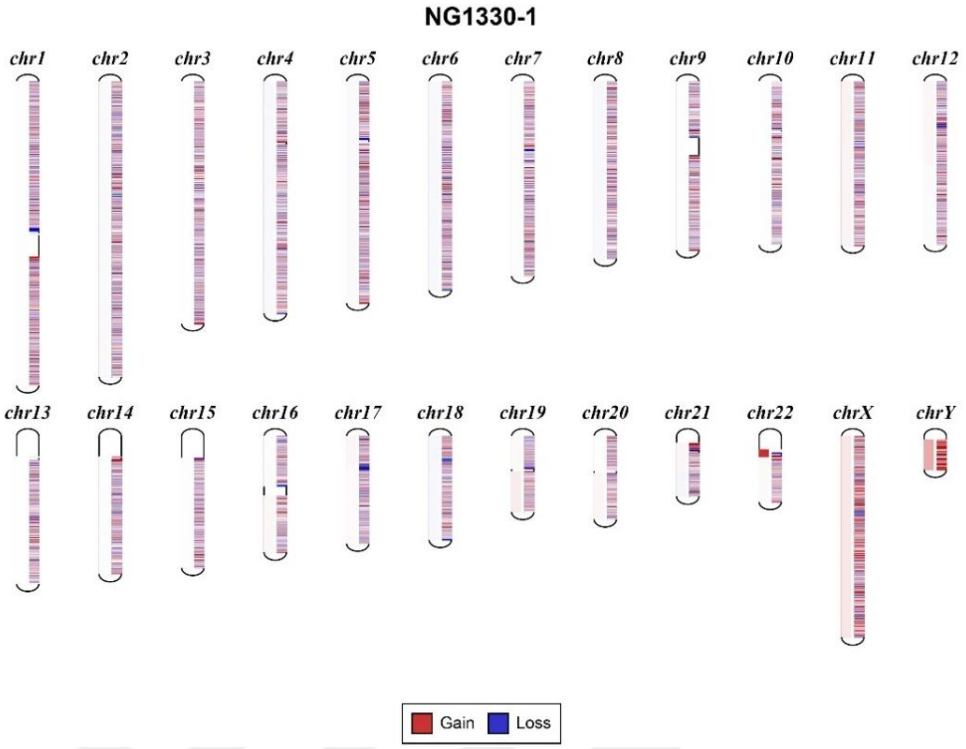

Figure 12. Genome-wide CNV profile of NG1330-1

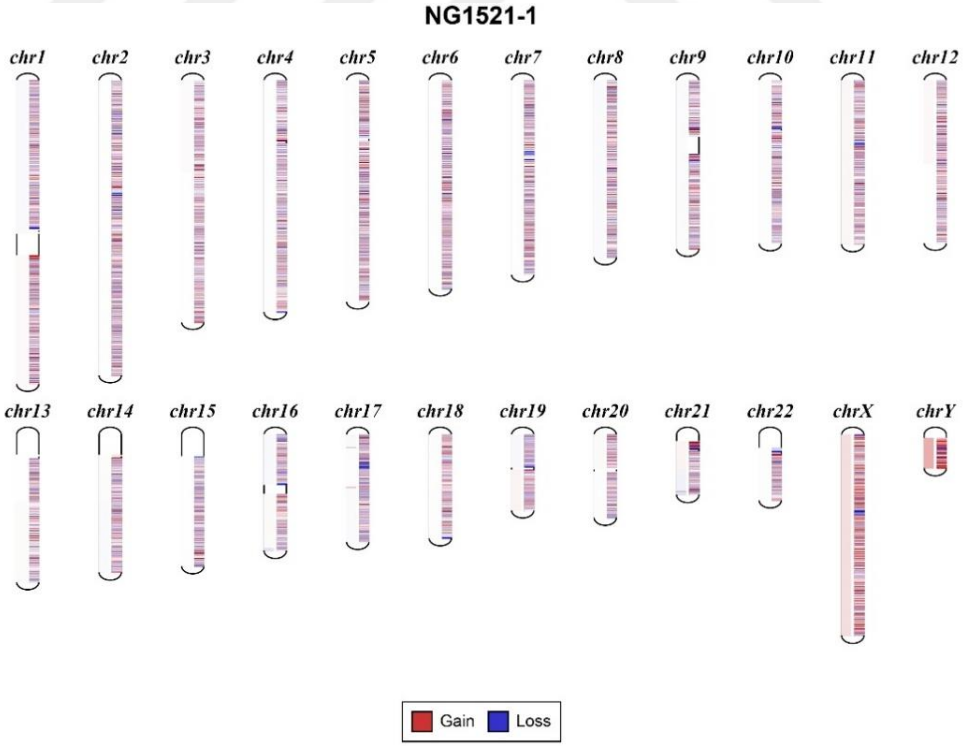

Figure 13. Genome-wide CNV profile of NG1521-1

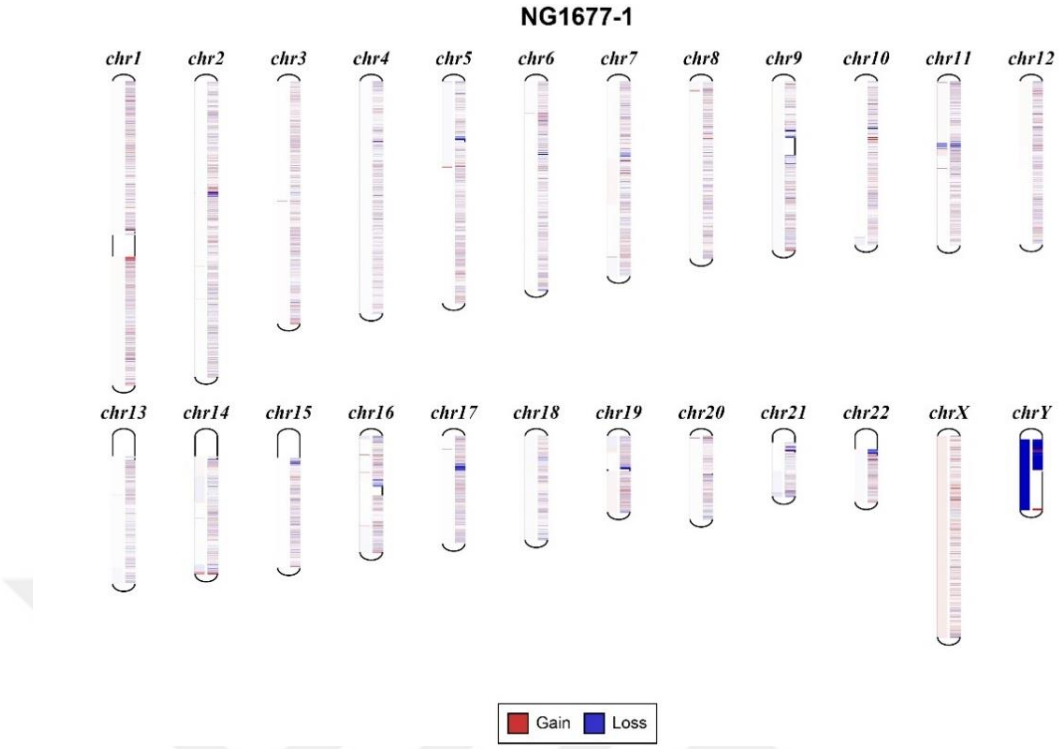

Figure 14. Genome-wide CNV profile of NG1677-1

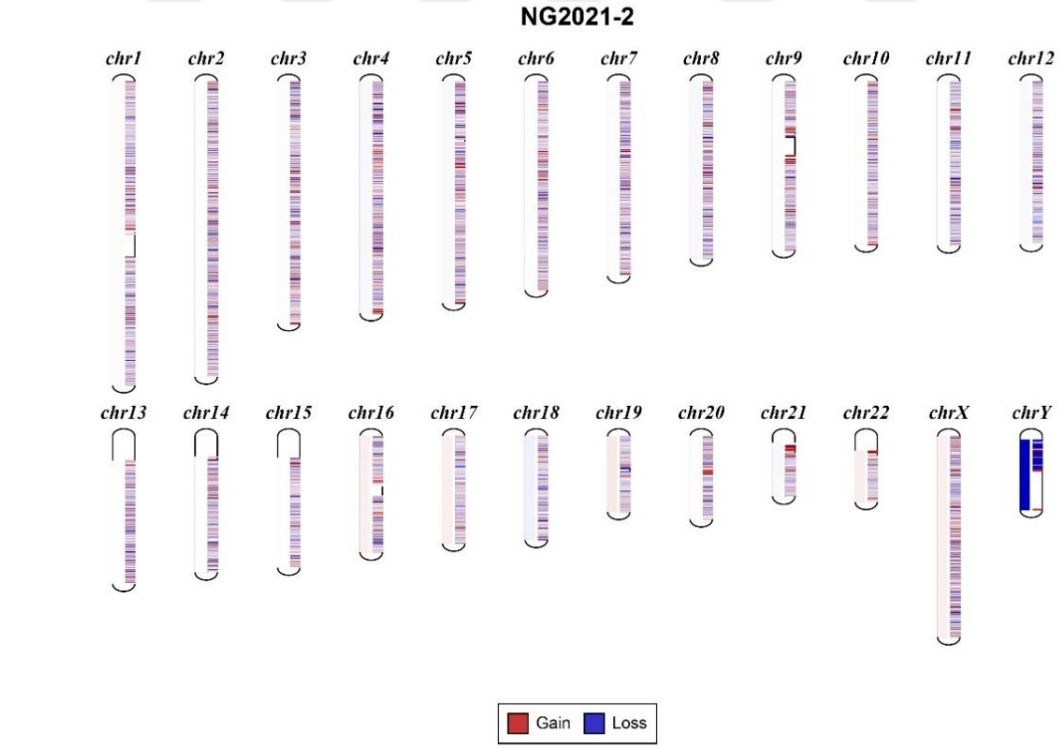

Figure 15. Genome-wide CNV profile of NG2021-2

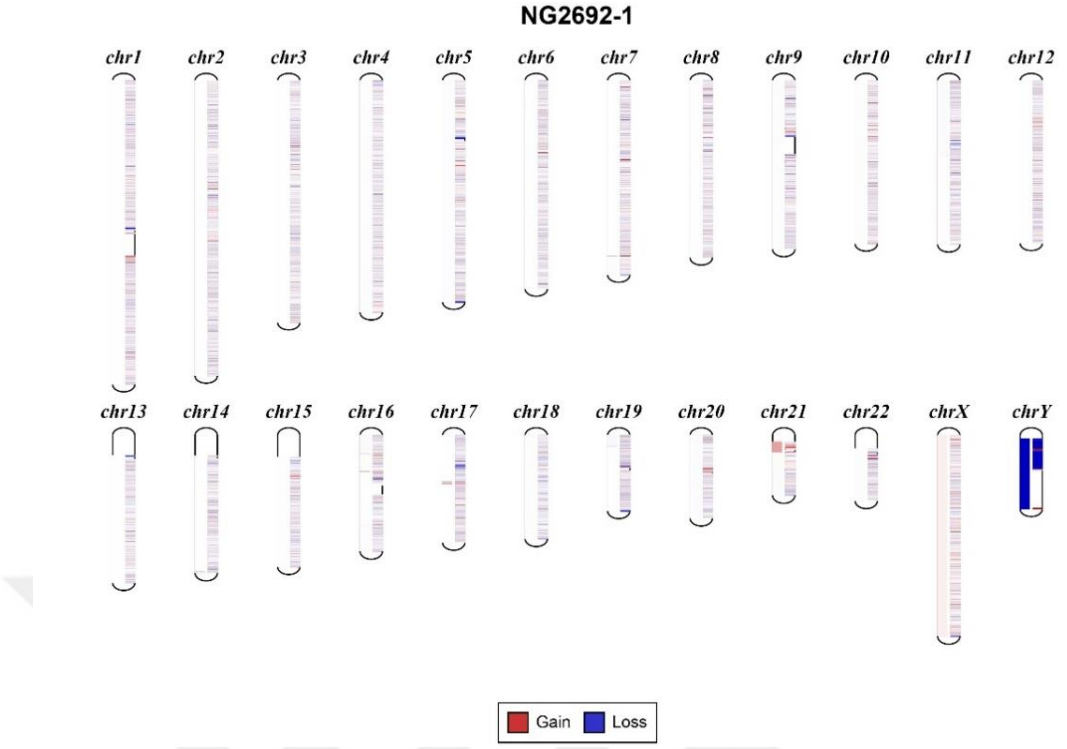

Figure 16. Genome-wide CNV profile of NG2692-1

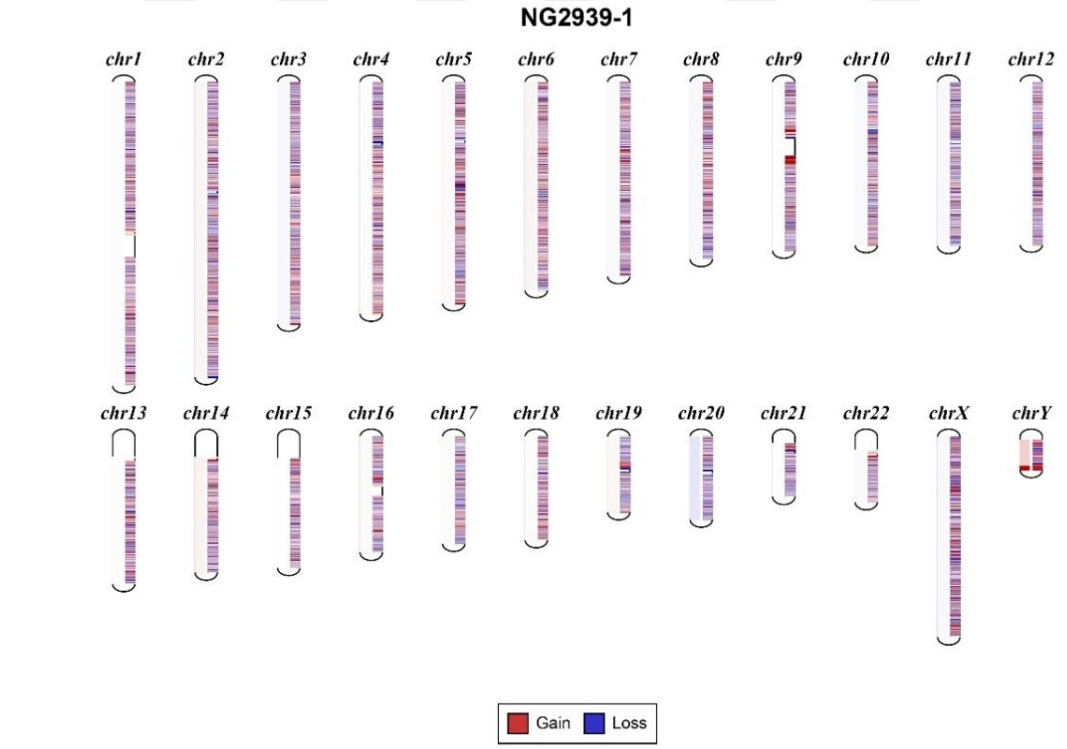

Figure 17. Genome-wide CNV profile of NG2939-1

Following structural variant detection using Manta and subsequent annotation with AnnotSV, no score-filtered pathogenic or likely pathogenic large-scale insertion, deletion, duplication, or inversion were identified in the cohort.

4.6 Integrative Functional Assessment of Candidate Genes

In cases lacking pathogenic variants in known MLIS-associated genes and without significant structural anomalies, a systematic evaluation was undertaken to identify and prioritize novel candidate genes. This section presents a comprehensive functional characterization of these candidates, integrating in silico predictions of variant deleteriousness, gene ontology and pathway enrichment analyses, as well as biological network context.

Table 14. Annotated results of the prioritized variant in NG958-1

<table>
<tr><th colspan="4">NG958-1</th></tr>
<tr><th>Variant Information</th><th>Population Allele Frequency</th><th>Pathogenicity Scores</th><th>Evolutionary Conservation</th></tr>
<tr><td>Gene: ARSD</td><td>gnomAD: 0</td><td>CADD: 22.1</td><td rowspan="3">GERP++: 3.08</td></tr>
<tr><td>Genomic position: GRCh38(chrX):g.2925688G>C</td><td>Iranome: 0</td><td>REVEL: 0.751</td></tr>
<tr><td>Alteration at the transcript level: NM_001669.4</td><td>UK biobank: 0</td><td>SIFT: 0.001</td></tr>
<tr><td>Molecular consequence: missense variant</td><td>1000G: 0</td><td>MutationTaster: 0.9999</td><td rowspan="3">phyloP: 7.442</td></tr>
<tr><td rowspan="2">Zygosity: hemizygous</td><td>Kaviar: 0</td><td rowspan="2">ACMG: Variant of Uncertain Significance</td></tr>
<tr><td>In-house Turkish sample cohort: 3</td></tr>
</table>

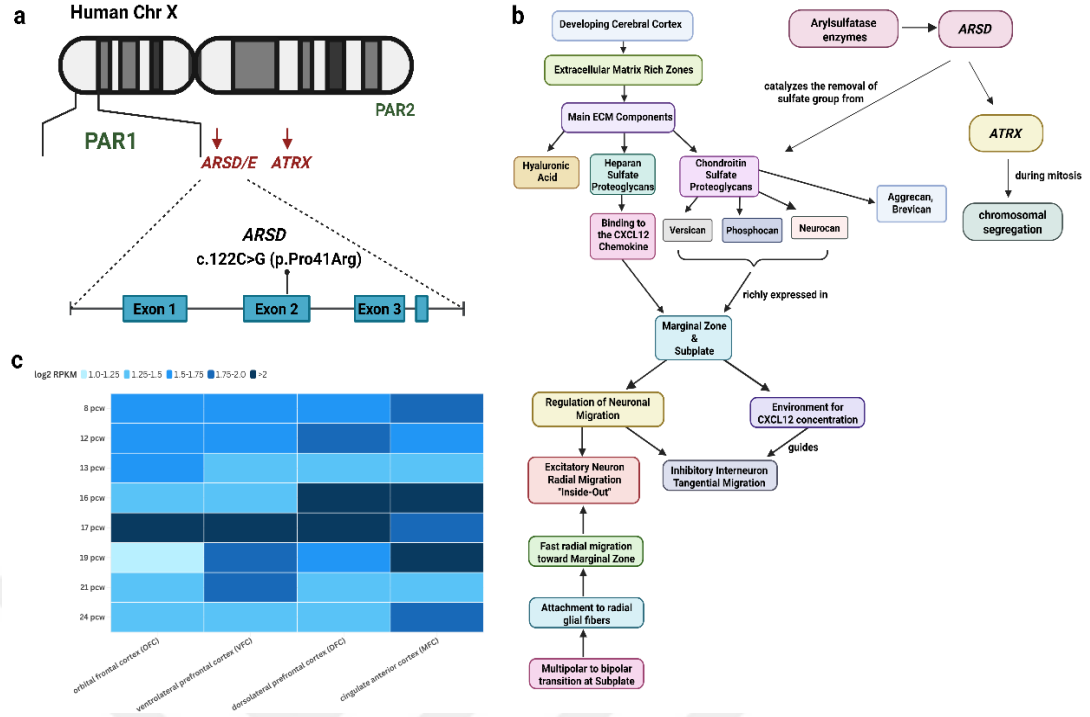

Figure 18. Schematic representation of the variant on the ARSD

a, Schematic representation of the variant on the *ARSD* (not to scale). b, Hypothetical functional pathway involving *ARSD* and its potential relevance to MLIS pathogenesis. c, Spatio-temporal distribution of *ARSD* expression across four cortical subregions of the developing human brain. Panels (a) and (b) were created in BioRender. Aral, M. (2025) https://BioRender.com/5werny1

Table 15. Annotated results of the prioritized variant in NG1521-1

NG1521-1			
Variant Information	**Population Allele Frequency**	**Pathogenicity Scores**	**Evolutionary Conservation**
Gene: *PACS2*	**gnomAD:** 0	**CADD:** 26	**GERP++:** 4.58
Genomic position: GRCh38(chr14):g.105381987A>G	**Iranome:** 0	**REVEL:** 0.095	
Alteration at the transcript level: NM_001100913.3	**UK biobank:** 0	**SIFT:** 0.197	
Molecular consequence: missense variant	**1000G:** 0	**MutationTaster:** 0.9999	**phyloP:** 7.086
Zygosity: heterozygous	**Kaviar:** 0	**ACMG:** Variant of Uncertain Significance	
	In-house Turkish sample cohort: 2		

Table 16. Annotated results of the prioritized variant in NG1521-1

NG1521-1			
Variant Information	**Population Allele Frequency**	**Pathogenicity Scores**	**Evolutionary Conservation**
Gene: *SPTAN1*	**gnomAD:** 0	**CADD:** 24.9	**GERP++:** 6.17
Genomic position: GRCh38(chr9):g.128618084A>C	**Iranome:** 0	**REVEL:** 0.429	
Alteration at the transcript level: NM_001130438.3	**UK biobank:** 0	**SIFT:** 0.1	
Molecular consequence: missense variant	**1000G:** 0	**MutationTaster:** 1	**phyloP:** 8.899
Zygosity: heterozygous	**Kaviar:** 0	**ACMG:** Variant of Uncertain Significance	
	In-house Turkish sample cohort: 1		

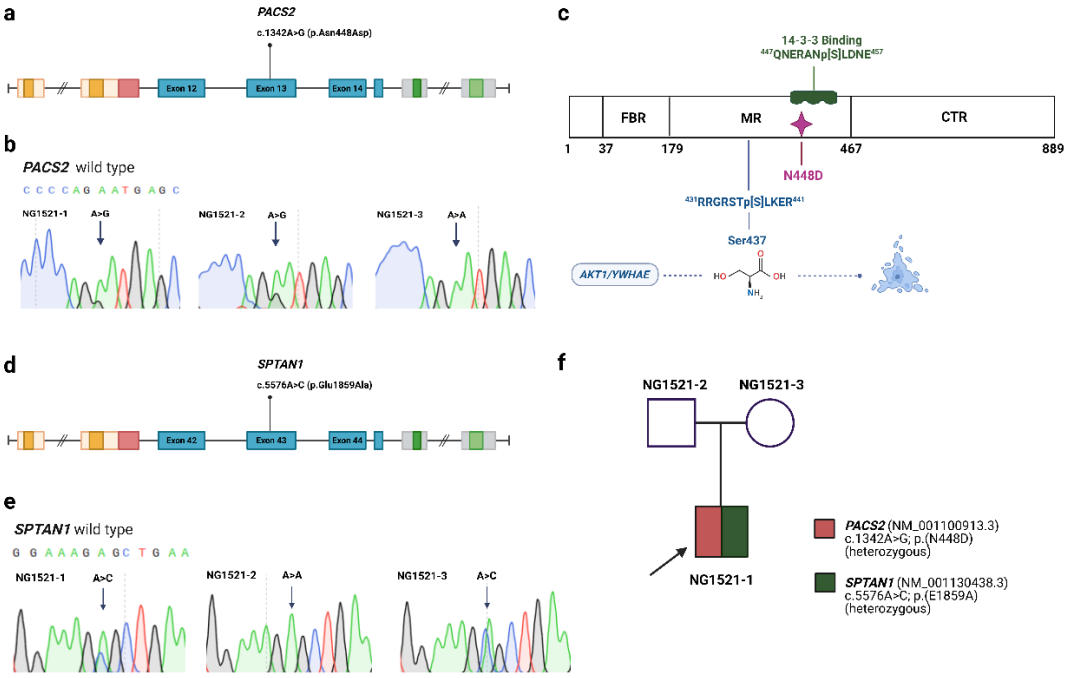

Figure 19. Schematic representation of the variant on the PACS2

a, Schematic representation of the variant on the *PACS2* (not to scale). b, Sanger sequencing validation of the c.1342A>G (p.Asn448Asp) variant. c, The N448D substitution is located in the middle region (MR) of PACS2, within a predicted 14-3-3 binding motif, suggesting a potential disruption of protein–protein interactions. Furin Binding Region (FBR, 37–179), Middle Region (MR, 179–467), C-terminal Region (CTR, 467–889). d, Schematic representation of the variant on the *SPTAN1* (not to scale). e, Sanger sequencing validation of the c.5576A>C (p.Glu1859Ala) variant. f, A blended phenotype is proposed based on the combined presence of these two variants for NG1521-1. Panels (a), (c), and (d) were created in BioRender. Aral, M. (2025) https://BioRender.com/yylrk7d

Table 17. Annotated results of the prioritized variant in NG2692-1

NG2692-1			
Variant Information	**Population Allele Frequency**	**Pathogenicity Scores**	**Evolutionary Conservation**
Gene: *KCNB1*	**gnomAD:** 0.00001505	**CADD:** 24	**GERP++:** 5.03
Genomic position: GRCh38(chr20):g.49373023C>A	**Iranome:** 0	**REVEL:** 0.693	
Alteration at the transcript level: NM_004975.4	**UK biobank:** 0	**SIFT:** 0.001	
Molecular consequence: missense variant	**1000G:** 0	**MutationTaster:** 1	**phyloP:** 5.169
Zygosity: homozygous	**Kaviar:** 0	**ACMG:** Variant of Uncertain Significance	
	In-house Turkish sample cohort: 3		

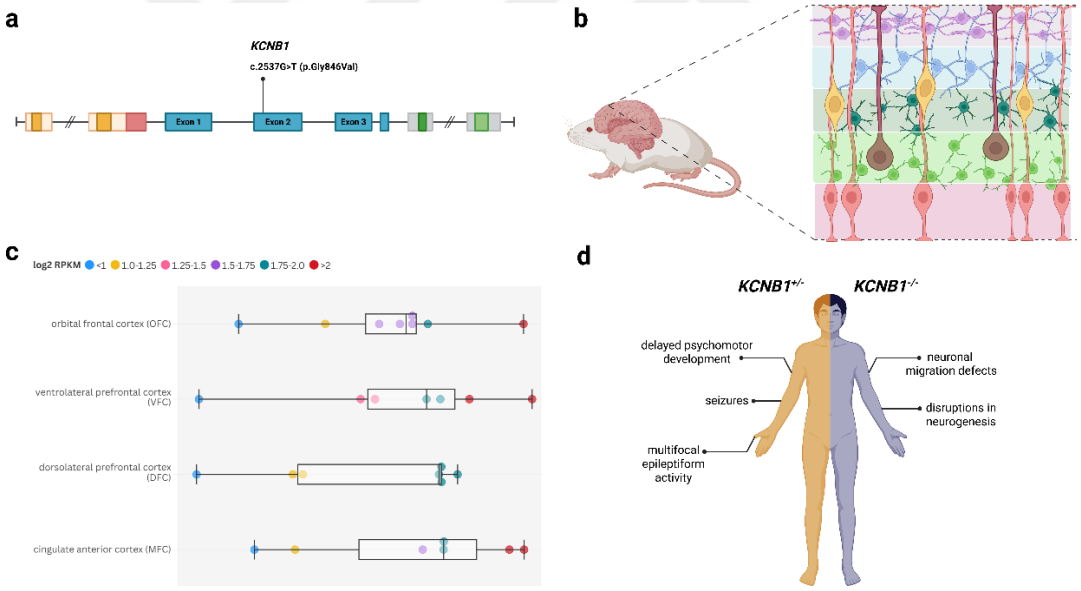

Figure 20. Schematic representation of the variant on the KCNB1

a, Schematic representation of the variant on the *KCNB1* (not to scale). b, Cortical layering in the developing mouse brain. c, Regional transcriptional profile of *KCNB1* across the developing human cerebral cortex. d, Proposed consequences of $KCNB1^{+}$ $/^{-}$ and $KCNB1^{-}$ $/^{-}$. Although monoallelic mutations may compromise potassium channel function and result in epilepsy-like behavior, biallelic loss is anticipated to cause profound neurodevelopmental disruptions, potentially culminating in severe cortical malformations. Panels (a), (b) and (d) were created in BioRender. Aral, M. (2025) https://BioRender.com/ewbk6nc

5 DISCUSSION

Rare NDDs associated with cortical malformations represent significant causes of morbidity and mortality, often leading to intellectual disability, autism spectrum disorders, and epilepsy, typically manifesting in infancy or early childhood.

The *PDCD6IP* variant identified in NG31-1 is a splice donor variant rather than a missense variant, suggesting a distinct mechanism of disruption compared to other alterations. The vast majority of splice-site mutations lead to either exon skipping or aberrant splice-site activation in both germline and somatic cells. These two outcomes can have markedly different phenotypic consequences, which are often difficult to predict, as most diagnostic gene screenings do not routinely incorporate RNA-level analyses from affected individuals and their families. To predict the likely molecular consequence of this variant, we employed the CRYP-SKIP tool, which estimated a high likelihood of exon skipping (PCR-E = 0.19) rather than cryptic splice-site activation (155). Given the length of the exon and its elevated EIE score (491.19), this region appears to be enriched in exonic splicing enhancers that are normally critical for accurate splicing. Exon skipping may disrupt these conserved enhancer motifs, potentially resulting in a frameshift or loss of essential protein domains. Such aberrant splicing could compromise *PDCD6IP* function either via nonsense-mediated mRNA decay (NMD) or by generating a truncated, non-functional protein.

In this specific transcript (NM_013374.6), which contains a total of 18 exons, the variant affects the canonical splice donor site at the 3′ end of exon 16. As exon 16 is 124 nucleotides long, its skipping is predicted to disrupt the reading frame. This frameshift would likely introduce a premature termination codon (PTC), most probably within or near exon 17. Since this PTC is located more than 50–55 nucleotides upstream of the final exon-exon junction, it is expected to trigger NMD (156). In such cases, if translation is prematurely terminated at a PTC located upstream of one or more exon junction complexes (EJCs), the remaining downstream EJCs serve as molecular markers of incomplete translation, thereby initiating the NMD pathway. In this case, the position of the predicted PTC satisfies the classical criteria for NMD

targeting, strongly suggesting that the transcript will be rapidly degraded, ultimately resulting in loss of *PDCD6IP* function.

We identified a heterozygous likely pathogenic missense variant in *ACTG1* in patient NG1225-1 and a similar variant in *ACTB* in patient NG2939-1, each observed only once within our in-house Turkish sample cohort and absent from public population databases. Both variants are highly diagnostic of Baraitser-Winter cerebrofrontofacial syndrome (BWCFF). While the classical neurological phenotype of BWCFF typically includes frontal or central pachygyria, our cases presented with severe lissencephaly and prenatal-onset microcephaly. These findings suggest that in rare instances, *ACTG1* and *ACTB* variants may underlie more severe cortical malformations within the BWCFF spectrum, expanding the known phenotypic range of the disorder (157).

DCX mutations are well-established causes of X-linked lissencephaly and subcortical band heterotopia (SBH), typically exhibiting sex-specific phenotypic presentations due to X-inactivation in females and hemizygous expression in males. In our male patient, NG1330-1, we observed a hemizygous missense variant in *DCX*. Although no neuroimaging data were available for this patient, the clinical diagnosis of lissencephaly is consistent with the classical phenotype observed in hemizygous males with *DCX* mutations.

Moreover, this patient also harbors a homozygous missense variant in *CNTN4*, a gene previously implicated in neuropsychiatric phenotypes. While the contribution of *CNTN4* to lissencephaly remains unclear, it is plausible that this variant may act as a genetic modifier, influencing the severity or spectrum of the phenotype. Given the absence of neuroimaging and the co-occurrence of potentially interacting variants, it is difficult to definitively attribute the phenotype to the *DCX* variant alone. Additionally, although male patients are generally expected to be non-mosaic for X-linked variants, post-zygotic mosaicism or epigenetic mechanisms could contribute to inter-individual variability and should remain a consideration in clinical interpretation.

Taken together, these findings highlight the complexity of variant interpretation in cases involving X-linked genes, particularly when additional rare homozygous mutations are present, and underscore the importance of integrating genomic, clinical, and ideally radiological data for accurate diagnosis.

We also identified a heterozygous pathogenic missense variant in *TUBA1A* in patient NG1677-1, a well-established gene associated with tubulinopathies, referred to as tubulin-related cortical dysgenesis. Among tubulinopathies, the core phenotype of *TUBA1A* is characterized by MLIS. This variant was detected only once in our in-house Turkish sample cohort and was absent from major public population databases, further reinforcing its rarity and pathogenicity. Disruption of *TUBA1A* function is therefore interpreted as genetically diagnostic and likely causative factor in our patient.

Although homozygous *PPFIBP1* is thought to be the primary genetic cause of cortical malformation in patient NG2021-2 due to its consistency with clinical findings, its relatively high allele frequency in population databases raises questions about reduced penetrance. Additionally, the co-occurrence of a homozygous *SMC4* variant in the same patient supports its potential role as a novel candidate gene, given its key function in the Condensin-II complex, and further, the Condensin-II:MCPH1 interaction during prophase chromosome condensation in the M phase (158).

To explore potential structural variant contributions to the etiology of MLIS, particular emphasis was placed on the 17p13.3 chromosomal region, with a primary focus on deletions encompassing the *PAFAH1B1* gene. While deletions causing MDS may vary in size from 0.1 to 2.9 Mb, they consistently involve *PAFAH1B1*. Structural variant detection in this study leveraged depth-of-coverage-based analysis, wherein genomic copy number changes are inferred from deviations in normalized read depth, expressed as $\log_2$ ratios. In a diploid genome, a balanced copy number yields a theoretical $\log_2$ ratio of zero, whereas a heterozygous deletion produces a ratio of $\log_2 (1/2) = -1$. Given the technical variability inherent to exome sequencing, such as GC-content bias and uneven capture efficiency, a more permissive threshold of -0.5 was employed, in line with established CNV detection standards. This approach

maximizes sensitivity while preserving specificity, particularly in challenging genomic regions. Across the 17p13.3 locus, including the critical *PAFAH1B1* region, no genomic segments demonstrated $\log_2$ ratio values below the defined deletion threshold. These findings argue against the presence of pathogenic heterozygous deletions involving *PAFAH1B1* or contiguous multi-gene deletions typically seen in MDS.

The robustness of this negative finding is further supported by the use of quantitatively validated detection parameters rather than a lack of sensitivity. Additionally, no pathogenic or likely pathogenic CNVs were identified elsewhere in the genome that could account for the phenotype via known microdeletion or microduplication syndromes. While small intragenic deletions or non-coding regulatory disruptions beyond current resolution limits cannot be entirely excluded, these results point toward a non-MDS disease mechanism, potentially implicating single-gene defects or subtle variants undetectable by CNV analysis.

In the later stage, to further narrow down the list of candidate genes, we focused on likely driver genes, their positions within functional interaction hierarchies, and their expression patterns in the developing human brain, as delineated by the Schaefer-Yeo parcellation of the cerebral cortex, rather than in the adult brain.

In patient NG958-1, *ARSD* emerges as a strong candidate gene potentially contributing to the pathogenesis of MLIS. *ARSD* encodes arylsulfatase D, a member of the sulfatase enzyme family, and is located on Xp22.3, just distal to the pseudoautosomal region 1 (PAR1), within a genomic cluster of arylsulfatase genes. Although *ARSD* has not been demonstrated to possess intrinsic sulfatase enzymatic activity, it retains a conserved N-terminal domain that is functionally critical in catalytically active sulfatases. Moreover, in contrast to its paralog *ARSE*, mutations in which cause chondrodysplasia punctata with associated microcephaly, *ARSD* is ubiquitously expressed, suggesting a broader physiological role. Notably, *ARSD* is among the subset of X-linked genes that escape X chromosome inactivation (XCI), implying that dosage sensitivity may be especially critical in hemizygous males. This

is particularly relevant in the context of neurodevelopment, where precise gene dosage is often essential for maintaining developmental gradients.

Intriguingly, recent transcriptomic studies in embryonic mouse models lacking the chromatin remodeler *ATRX* have shown significant downregulation of *ARSD* in the forebrain. *ATRX* mutations are known to cause syndromes characterized by microcephaly and lissencephaly, implicating *ARSD* within a transcriptional regulatory network essential for cortical development. Furthermore, the coordinated downregulation of other ancestral PAR genes in *ATRX*-deficient tissue provides additional support for *ARSD*'s involvement in early brain patterning (159).

Mounting evidence from experimental neurobiology underscores the critical role of sulfated glycosaminoglycans (GAGs), particularly chondroitin sulfate (CS) and heparan sulfate (HS), in orchestrating neuronal migration during corticogenesis. These molecules are highly enriched in the marginal zone and subplate, which serve as key migratory scaffolds for both radial and tangentially migrating neurons (160). Perturbations in the degree or spatial patterning of GAG sulfation have been shown to disrupt layer-specific neuronal positioning, affecting both excitatory and inhibitory lineages (161).

Given *ARSD*'s identity as a sulfatase family member, it is plausible that a pathogenic variant might compromise the sulfation homeostasis of ECM-bound CS or HS chains. Such dysregulation could interfere with the finely tuned spatiotemporal cues required for proper neuronal migration. This mechanistic framework is substantiated by in vitro studies demonstrating that alterations in CS sulfation, whether excessive, deficient, or spatially mislocalized, lead to disrupted migratory trajectories and disorganized laminar architecture, features reminiscent of MLIS.

In conclusion, *ARSD* represents a biologically and mechanistically compelling candidate for MLIS. Its evolutionary origin, status as an XCI escape, putative regulation by *ATRX*, and likely role in ECM-mediated signaling converge to implicate it in key processes governing cortical development. The phenotype observed in our

patient may stem from perturbed neuronal migration due to altered ECM sulfation landscapes, establishing a potential link between *ARSD* dysfunction and cortical malformations.

In patient NG1521-1, we propose *PACS2* as a candidate gene potentially contributing to the observed cortical malformations. A heterozygous (paternal origin) missense variant (N448D) was identified within the *PACS2* gene. This variant lies directly within a canonical 14-3-3 binding motif in the middle region (MR) of *PACS2*, a domain essential for mediating protein-protein interactions and regulating subcellular localization.

The N448D substitution may interfere with phospho-dependent binding of 14-3-3 proteins, particularly *YWHAE* (14-3-3ε), which interacts with phosphorylated Ser437 in the adjacent region. This site is thought to be regulated by *AKT1* and plays a role in modulating *PACS2*'s apoptotic and trafficking functions during mitotic progression.

Support for *PACS2*'s role in neurodevelopmental pathogenesis comes from previously reported cases of a recurrent *PACS2*-E209K mutation, which causes early-onset epileptic encephalopathy (162). Functional studies of this mutation have shown that it prolongs the half-life of the *PACS2* protein, enhances its interaction with 14-3-3ε, and increases cellular susceptibility to apoptosis. Interestingly, the E209 residue lies outside of the canonical 14-3-3 binding motifs, suggesting an indirect effect. In contrast, the N448D variant in our patient occurs within the core binding interface and is thus more likely to disrupt, rather than enhance, 14-3-3 interaction.

This mechanistic contrast between E209K and N448D may explain the phenotypic variability observed across PACS2-associated disorders. While both variants affect the PACS2:14-3-3 signaling axis, they appear to exert opposing effects, one increasing and the other decreasing 14-3-3 binding, leading to divergent outcomes such as epilepsy, autism, or cortical malformations. These findings underscore the importance of variant-specific functional consequences in PACS2-related pathogenesis and

support the hypothesis that both gain and loss of 14-3-3 interactions can perturb neurodevelopment.

In addition to the paternally inherited heterozygous *PACS2* variant, a maternally inherited heterozygous *SPTAN1* variant also emerges as a candidate potentially contributing to the progressive microcephaly phenotype (MIM #613477) observed in the same patient. This variant has not been previously reported in literature databases and is currently classified as a variant of uncertain significance (VUS) based on ACMG guidelines. The presence of two inherited heterozygous variants, each from an unaffected parent, raises the possibility of reduced penetrance, which may account for the cortical malformations in the proband (163). Notably, this observation supports the concept of intrafamilial phenotypic variability, wherein even deleterious variants may result in a very mild or subclinical phenotype, or no phenotype at all, in some carriers.

We also recognise the possibility of a blended phenotype in NG1521-1. Even well-characterized variants can lead to unpredictable outcomes in the context of a complex genetic background, and this challenge becomes even more pronounced when dealing with variants of uncertain significance or those with incomplete penetrance. However, in a large clinical WES cohort, approximately 5% of diagnosed cases were found to have pathogenic variants in two distinct disease-causing genes (164). Similarly, a study of patients from consanguineous families reported dual molecular diagnoses in 1 out of 18 cases (165). These findings underscore the importance of considering multilocus contributions when evaluating complex neurodevelopmental phenotypes.

In patient NG2692-1, we identified a homozygous missense variant in *KCNB1* in a single patient from our Turkish sample cohort, in whom no other individual harbored this variant in a homozygous state. While *KCNB1* is classically associated with autosomal dominant developmental and epileptic encephalopathy, our findings offer a new plausible avenue for a distinct autosomal recessive mechanism contributing to cortical malformations. Functional studies in knockout mouse models have demonstrated that *KCNB1* plays a key role in neuronal migration, as glutamatergic

neurons fail to reach upper cortical layers and accumulate abnormally in deeper zones (166). This migratory defect has been linked to impaired function of Integrin-K+ channel complexes, of which *KCNB1* is a central component. Moreover, loss of *KCNB1* disrupts integrin-mediated PI3K/Akt signaling pathways that are crucial for neural progenitor proliferation (167,168). Taken together, these data suggest that homozygous disruption of *KCNB1* may impair both neurogenesis and neuronal migration, supporting its candidacy as a novel autosomal recessive gene implicated in cortical development.

6 CONCLUSION

No matter how serious and compelling the concern in “rare human diseases”, science and medicine should make a concerted effort to collaborate on understanding undiagnosed complex disorders and their treatment. We are witnessing a transformative era fueled by advances in NGS technologies, which now allow for the detection of previously inaccessible pathological variants. However, the cumulative prevalence of such pathologies is projected to increase globally with time. Translating this approach into a collective will not be as rare as universally perceived.

Our hope is that the current gap in this specific area will be at least partially bridged, both through the expansion of clinical knowledge and the increasing accessibility of advanced diagnostic tools. Furthermore, a well-established correlation between genetic variants and phenotypic presentations may yield deeper insights into the underlying mechanisms contributing to disease incidence.

Within this framework, we have conducted NGS-guided data assessment to identify causal genes and investigate possible mechanisms of MLIS, which falls under the umbrella of MCD. Through human genomics data, we characterized disease-causing mutations and expanded the phenotypic spectrum and potential mechanisms for each MLIS patient in our cohort.

Further in vitro studies are warranted to validate these proposed mechanisms and elucidate the broader functional roles of novel candidate genes in NDDs. In particular, state-of-the-art organoid models will be essential in recapitulating disease-relevant physiology and enabling mechanistic exploration at the cellular level.

7 REFERENCES

1. Kuzniecky R. (2015). Epilepsy and malformations of cortical development: new developments. *Current opinion in neurology*, *28*(2), 151–157.
2. Soden, S. E., Saunders, C. J., Willig, L. K., Farrow, E. G., Smith, L. D., Petrikin, J. E., LePichon, J. B., Miller, N. A., Thiffault, I., Dinwiddie, D. L., Twist, G., Noll, A., Heese, B. A., Zellmer, L., Atherton, A. M., Abdelmoity, A. T., Safina, N., Nyp, S. S., Zuccarelli, B., Larson, I. A., … Kingsmore, S. F. (2014). Effectiveness of exome and genome sequencing guided by acuity of illness for diagnosis of neurodevelopmental disorders. *Science translational medicine*, *6*(265), 265ra168.
3. Layo-Carris, D. E., Lubin, E. E., Sangree, A. K., Clark, K. J., Durham, E. L., Gonzalez, E. M., Smith, S., Angireddy, R., Wang, X. M., Weiss, E., Toutain, A., Mendoza-Londono, R., Dupuis, L., Damseh, N., Velasco, D., Valenzuela, I., Codina-Solà, M., Ziats, C., Have, J., Clarkson, K., … Bryant, L. M. (2024). Expanded phenotypic spectrum of neurodevelopmental and neurodegenerative disorder Bryant-Li-Bhoj syndrome with 38 additional individuals. *European journal of human genetics : EJHG*, *32*(8), 928–937.
4. Dehay, C., Kennedy, H., & Kosik, K. S. (2015). The outer subventricular zone and primate-specific cortical complexification. *Neuron*, *85*(4), 683–694.
5. Zaghi, M., Banfi, F., Bellini, E., & Sessa, A. (2021). Rare Does Not Mean Worthless: How Rare Diseases Have Shaped Neurodevelopment Research in the NGS Era. *Biomolecules*, *11*(11), 1713.
6. Knight G. T., Lundin B. F., Iyer N., Lydia M., Ashton T., Sethares W. A., et al. (2018). Engineering induction of singular neural rosette emergence within hpsc-derived tissues. eLife 7, e37549. 10.7554/eLife.37549
7. Fedorova V, Vanova T, Elrefae L, Pospisil J, Petrasova M, Kolajova V, Hudacova Z, Baniariova J, Barak M, Peskova L, Barta T, Kaucka M, Killinger M, Vecera J, Bernatik O, Cajanek L, Hribkova H, Bohaciakova D. Differentiation of neural rosettes from human pluripotent stem cells in vitro is sequentially regulated on a molecular level and accomplished by the mechanism reminiscent of secondary neurulation. Stem Cell Res. 2019 Oct;40:101563.
8. Cadwell, C. R., Bhaduri, A., Mostajo-Radji, M. A., Keefe, M. G., & Nowakowski, T. J. (2019). Development and Arealization of the Cerebral Cortex. *Neuron*, *103*(6), 980–1004.
9. Takahashi, T., Nowakowski, R. S., & Caviness, V. S., Jr (1996). The leaving or Q fraction of the murine cerebral proliferative epithelium: a general model of neocortical neuronogenesis. *The Journal of neuroscience : the official journal of the Society for Neuroscience*, *16*(19), 6183–6196.
10. Cai, L., Hayes, N. L., Takahashi, T., Caviness, V. S., Jr, & Nowakowski, R. S. (2002). Size distribution of retrovirally marked lineages matches prediction from population measurements of cell cycle behavior. *Journal of neuroscience research*, *69*(6), 731–744.
11. Fietz SA, Kelava I, Vogt J, Wilsch-Brauninger M, Stenzel D, Fish JL, Corbeil D,Riehn A,Distler W,NitschR,etal. 2010.OSVZ progenitors of human and ferret neocortex are epithelial-like and expand by in tegrin signaling. Nat Neurosci 13: 690–699.

12. Hansen D, Lui J, Parker P, Kriegstein A. 2010. Neurogenic radial glia in the outer subventricular zone of human neocortex. Nature 464: U554–U110.
13. Reillo I, de Juan Romero C, Garcia-Cabezas MA, Borrell V. 2011. A role for intermediate radial glia in the tangential expansion of the mam malian cerebral cortex. Cereb Cortex 21: 1674–1694.
14. Thomsen, E., Mich, J., Yao, Z. *et al*. Fixed single-cell transcriptomic characterization of human radial glial diversity. *Nat Methods* **13**, 87–93 (2016).
15. Ostrem, B., Di Lullo, E., & Kriegstein, A. (2017). oRGs and mitotic somal translocation - a role in development and disease. *Current opinion in neurobiology*, *42*, 61–67.
16. Norden C, Young S, Link BA, Harris WA. 2009. Actomyosin is the main driver of interkinetic nuclear migration in the retina. Cell 138: 1195–1208.
17. SchenkJ,Wilsch-Brauninger M,CalegariF,HuttnerWB.2009.MyosinII is required for interkinetic nuclear migration of neural progenitors. Proc Natl Acad Sci 106: 16487–16492.
18. Matsuzaki, F., & Shitamukai, A. (2015). Cell Division Modes and Cleavage Planes of Neural Progenitors during Mammalian Cortical Development. *Cold Spring Harbor perspectives in biology*, *7*(9), a015719.
19. Meyer EJ, Ikmi A, Gibson MC. 2011. Interkinetic nuclear migration is a broadly conserved feature of cell division in pseudostratified epithelia. Curr Biol 21: 485–491.
20. Tsai JW,LianWN,KemalS,KriegsteinAR,ValleeRB.2010.Kinesin3and cytoplasmic dynein mediate interkinetic nuclear migration in neural stem cells. Nat Neurosci 13: 1463–1471.
21. Ostrem, B. E., Lui, J. H., Gertz, C. C., & Kriegstein, A. R. (2014). Control of outer radial glial stem cell mitosis in the human brain. *Cell reports*, *8*(3), 656–664.
22. Jamuar, S. S., & Walsh, C. A. (2015). Genomic variants and variations in malformations of cortical development. *Pediatric clinics of North America*, *62*(3), 571–585.
23. Noctor, S. C., Martinez-Cerdeno, V., Ivic, L. & Kriegstein, A. R. Cortical neurons arise in symmetric and asymmetric division zones and migrate through specific phases. Nat. Neurosci. 7, 136–144 (2004).
24. Haubensak, W., Attardo, A., Denk, W. & Huttner, W. B. Neurons arise in the basal neuroepithelium of the early mammalian telencephalon: a major site of neurogenesis. Proc. Natl Acad. Sci. USA 101, 3196–3201 (2004).
25. Nadarajah, B., & Parnavelas, J. G. (2002). Modes of neuronal migration in the developing cerebral cortex. *Nature reviews. Neuroscience*, *3*(6), 423–432.
26. Nadarajah, B., Alifragis, P., Wong, R. O. & Parnavelas, J. G. Ventricle-directed migration in the developing cerebral cortex. Nature Neurosci. 5, 218–224 (2002).
27. Nadarajah, B., Brunstrom, J. E., Grutzendler, J., Wong, R. O. & Pearlman, A. L. Two modes of radial migration in early development of the cerebral cortex. Nature Neurosci. 4, 143–150 (2001).
28. Leventer, R. J., Cardoso, C., Ledbetter, D. H. & Dobyns, W. B. LIS1: from cortical malformation to essential protein of cellular dynamics. Trends Neurosci. 24, 489–492 (2001).
29. Wynshaw-Boris, A. & Gambello, M. J. LIS1 and dynein motor function in neuronal migration and development. Genes Dev. 15, 639–651 (2001).

30. Parrini E, Conti V, Dobyns WB, Guerrini R. Genetic basis of brain malformations. Mol Syndromol. 2016;7(4):220-233.
31. Guerrini R, Dobyns WB. Malformations of cortical development: clinical features and genetic causes. Lancet Neurol. 2014;13(7):710-726.
32. Sir JH, Barr AR, Nicholas AK, et al. A primary microcephaly protein complex forms a ring around parental centrioles. Nat Genet. 2011;43(11):1147-1153.
33. Gilmore EC, Walsh CA. Genetic causes of microcephaly and lessons for neuronal development. Wiley Interdiscip Rev Dev Biol. 2013 Jul;2(4):461–78.
34. Blümcke I, Thom M, Aronica E, Armstrong DD, Vinters HV, Palmini A, et al. The clinicopathologic spectrum of focal cortical dysplasias: a consensus classification proposed by an ad hoc Task Force of the ILAE Diagnostic Methods Commission. Epilepsia 2011; 52: 158–74.
35. Desikan, R. S., & Barkovich, A. J. (2016). Malformations of cortical development. *Annals of neurology*, *80*(6), 797–810.
36. Sheen VL, Dixon PH, Fox JW, et al. Mutations in the X-linked filamin 1 gene cause periventricular nodular heterotopia in males as well as in females. Hum Mol Genet. 2001;10(17):1775-1783.
37. Haverfield EV, Whited AJ, Petras KS, Dobyns WB, Das S. Intragenic deletions and duplications of the LIS1 and DCX genes: a major disease causing mechanism in lissencephaly and subcortical band heterotopia. Eur J Hum Genet. 2009;17(7):911-918.
38. Delatycki, M., Leventer, R. Listen carefully: *LIS1* and *DCX* MLPA in lissencephaly and subcortical band heterotopia. *Eur J Hum Genet* **17**, 701–702 (2009).
39. Dobyns, W. B., Kirkpatrick, J. B., Hittner, H. M., Roberts, R. M., & Kretzer, F. L. (1985). Syndromes with lissencephaly. II: Walker-Warburg and cerebro-oculo-muscular syndromes and a new syndrome with type II lissencephaly. *American journal of medical genetics*, *22*(1), 157–195.
40. Devisme L, Bouchet C, Gonzalès M, Alanio E, Bazin A, Bessières B, et al. Cobblestone lissencephaly: neuropathological subtypes and correlations with genes of dystroglycanopathies. Brain 2012; 135: 469–82.
41. Barkovich AJ, Kuzniecky RI, Jackson GD, et al: A developmental and genetic classification for malformations of cortical development. Neurology 65:1873-1887, 2005
42. Barkovich AJ: Paediatric Neuroimaging (ed 4). Philadelphia, Lippincott Williams & Wilkins, 2005.
43. Stutterd CA, Leventer RJ.. Polymicrogyria: a common and heterogeneous malformation of cortical development. Am J Med Genet C Semin Genet 2014; 166C: 227–39.
44. Takanashi J, Barkovich AJ.. The changing MR imaging appearance of polymicrogyria: a consequence of myelination. AJNR Am J Neuroradiol 2003; 24: 788–93.
45. Barkovich AJ, Gressens P, Evrard P. Formation, maturation, and disorders of brain neocortex. Am J Neuroradiol 1992; 13:423^46.
46. Mischel PS, Nguyen LP, Vinters HV Cerebral cortical dysplasia associated with pediatric epilepsy. Review of neuropathologic features and proposal for a grading system. / Neuropath Exp Neurol 1995;54:137-153.

47. Barkovich AJ, Kuzniecky RI, Jackson GD, et al: Classification system for malformations of cortical development: Update 2001. Neurology 57: 2168-2178, 2001.
48. Granata T, Battaglia G, D'Incerti L, et al: Schizencephaly: Clinical findings, in Guerrini R, Andermann F, Canapicchi R (eds): Dysplasias of Cerebral Cortex and Epilepsy. Philadelphia, Lippincott-Raven, 1996, pp 407-415.
49. Raybaud C, Widjaja E.. Development and dysgenesis of the cerebral cortex: malformations of cortical development. Neuroimaging Clin N Am 2011; 21: 483–543.
50. Dies KA, Bodell A, Hisama FM, et al. Schizencephaly: Association With Young Maternal Age, Alcohol Use, and Lack of Prenatal Care. J Child Neurol. 2013;28:198–203.
51. Chong JX, Buckingham KJ, Jhangiani SN, et al. 2015. The genetic basis of Mendelian phenotypes: discoveries, challenges, and opportunities. Am. J. Hum. Genet. 97:199–215.
52. Wright, C.F.; FitzPatrick, D.R.; Firth, H.V. Paediatric genomics: Diagnosing rare disease in children. Nat. Rev. Genet. 2018, 19, 253–268.
53. Tong N. Priority Diseases and Reasons for Inclusion. In: Priority Medicines for Europe and the World 2013 Update. World Health Organization Publisher, Geneva, Switzerland, 2013.
54. Parenti, I.; Rabaneda, L.G.; Schoen, H.; Novarino, G. Neurodevelopmental Disorders: From Genetics to Functional Pathways. Trends Neurosci. 2020, 43, 608–621.
55. Mitchell K. J. (2011). The genetics of neurodevelopmental disease. *Current opinion in neurobiology*, *21*(1), 197–203.
56. Costanzo M., Kuzmin E., van Leeuwen J., Mair B., Moffat J., Boone C., Andrews B. Global Genetic Networks and the Genotype-to-Phenotype Relationship. Cell. 2019;177:85–100.
57. Davidson B.A., Hassan S., Garcia E.J., Tayebi N., Sidransky E. Exploring genetic modifiers of Gaucher disease: The next horizon. Hum. Mutat. 2018;39:1739–1751.
58. Barkovich AJ, Ferriero DM, Barr RM, et al: Microlissencephaly: A heterogeneous malformation ofcortical development. Neuropediatrics 29: 113-119, 1998.
59. Ashwal S, Michelson D, Plawner L, Dobyns WB. Practice parameter: Evaluation of the child with microcephaly (an evidence-based review): re port of the Quality Standards Subcommittee of the American Academy of Neurology and the Practice Committee of the Child Neurology Society. Neurology. 2009;73(11):887-897.
60. Dobyns WB. Primary microcephaly: new approaches for an old disorder. Am J Med Genet. 2002;112(4):315-317.
61. Woods CG, Parker A. Investigating microcephaly. Arch Dis Child. 2013;98(9):707-713.
62. Natacci, F., Bedeschi, M.F., et al., 2007. Norman-Roberts syndrome: characterization of the phenotype in early fetal life. Prenat. Diagn. 27 (6), 568e572.
63. Verrotti, A., Spalice, A., et al., 2010. New trends in neuronal migration disorders. Eur. J. Paediatr. Neurol. 14 (1), 1e12.
64. Chiba, E., Kimura, Y., Shimizu-Motohashi, Y., Miyagawa, N., Ota, M., Shigemoto, Y., Ohnishi, M., Nakaya, M., Nakagawa, E., Sasaki, M., & Sato, N. (2022). Clinical and neuroimaging findings in

patients with lissencephaly/subcortical band heterotopia spectrum: a magnetic resonance conventional and diffusion tensor study. Neuroradiology, 64(4), 825–836.

65. Alcantara, D., O'Driscoll, M., 2014. Congenital microcephaly. Am. J. Med. Genet. C Semin. Med. Genet. 166C, 124e139.
66. Zaqout, S., Morris-Rosendahl, D., Kaindl, A.M., 2017. Autosomal recessive primary microcephaly (MCPH): an update. Neuropediatrics 48, 135e142.
67. Jayaraman, D., Bae, B.-I., Walsh, C.A., 2018. The genetics of primary microcephaly. Annu. Rev. Genom. Hum. Genet. 19, 177e200.
68. Khetarpal, P., Das, S., Panigrahi, I., Munshi, A., 2016. Primordial dwarfism: overview of clinical and genetic aspects. Mol. Genet. Genom. 291, 1e15.
69. O'Neill, R.S., Schoborg, T.A., Rusan, N.M., 2018. Same but different: pleiotropy in centrosome-related microcephaly. Mol. Biol. Cell 29, 241e246.
70. Bakircioglu, M., et al., 2011. The essential role of centrosomal NDE1 in human cerebral cortex neurogenesis. Am. J. Hum. Genet. 88, 523e535.
71. Alkuraya, F.S., Cai, X., Emery, C., Mochida, G.H., Al-Dosari, M.S., Felie, J.M., Hill, R.S., Barry, B.J., Partlow, J.N., Gascon, G.G., Kentab, A., Jan, M., Shaheen, R., Feng, Y., Walsh, C.A., 2011. Human mutations in NDE1 cause extreme microcephaly with lissencephaly. Am. J. Hum. Genet. 88, 536e547.
72. Bond, J., et al., 2005. A centrosomal mechanism involving CDK5RAP2 and CENPJ controls brain size. Nat. Genet. 37, 353e355.
73. Yigit, G., Brown, K.E., Kayserili, H., Pohl, E., Caliebe, A., Zahnleiter, D., Rosser, E., Bögershausen, N., Uyguner, Z.O., Altunoglu, U., Nürnberg, G., Nürnberg, P., Rauch, A., Li, Y., Thiel, C.T., Wollnik, B., 2015. Mutations in CDK5RAP2 cause Seckel syndrome. Mol. Genet. Genomic. Med. 3, 467e480.
74. Létard, P., et al., 2018. Autosomal recessive primary microcephaly due to ASPM mutations: An update. Hum. Mutat. 39, 319e332.
75. Fish, J.L., Kosodo, Y., Enard, W., Pääbo, S., Huttner, W.B., 2006. Aspm specifically maintains symmetric proliferative divisions of neuroepithelial cells. Proc. Natl. Acad. Sci. U.S.A. 103, 10438e10443.
76. Megraw, T.L., Sharkey, J.T., Nowakowski, R.S., 2011. Cdk5rap2 exposes the centrosomal root of microcephaly syndromes. Trends Cell Biol. 21, 470e480.
77. Lizarraga, S.B., Margossian, S.P., Harris, M.H., Campagna, D.R., Han, A.P., Blevins, S., Mudbhary, R., Barker, J.E., Walsh, C.A., Fleming, M.D., 2010. Cdk5rap2 regulates centrosome function and chromosome segregation in neuronal progenitors. Development 137, 1907e1917.
78. Feng, Y., Walsh, C.A., 2004. Mitotic spindle regulation by Nde1 controls cerebral cortical size. Neuron 44, 279e293.
79. Kumar, A., Girimaji, S.C., Duvvari, M.R., Blanton, S.H., 2009. Mutations in STIL, encoding a pericentriolar and centrosomal protein, cause primary microcephaly. Am. J. Hum. Genet. 84, 286e290.

80. Patwardhan, D., Mani, S., Passemard, S., Gressens, P., Ghouzzi El, V., 2018. STIL balancing primary microcephaly and cancer. Cell Death Dis. 9, 65
81. Bazzi, H., Anderson, K.V., 2014. Acentriolar mitosis activates a p53-dependent apoptosis pathway in the mouse embryo. Proc. Natl. Acad. Sci. U.S.A 111, E1491eE1500.
82. Verloes, A., Drunat, S., Gressens, P., et al., 2009. Primary autosomal recessive microcephalies and seckel syndrome spectrum disorders. In: Adam, M.P., Ardinger, H.H., Pagon, R.A., et al. (Eds.), GeneReviews [Internet]. University of Washington, Seattle.
83. Higgins, J., Midgley, C., Bergh, A.-M., Bell, S.M., Askham, J.M., Roberts, E., Binns, R.K., Sharif, S.M., Bennett, C., Glover, D.M., Woods, C.G., Morrison, E.E., Bond, J., 2010. Human ASPM participates in spindle organisation, spindle orientation and cytokinesis. BMC Cell Biol. 11, 85.
84. Pulvers, J.N., Bryk, J., Fish, J.L., Wilsch-Bräuninger, M., Arai, Y., Schreier, D., Naumann, R., Helppi, J., Habermann, B., Vogt, J., Nitsch, R., Tóth, A., Enard, W., Pääbo, S., Huttner, W.B., 2010. Mutations in mouse Aspm (abnormal spindle-like microcephaly associated) cause not only microcephaly but also major defects in the germline. Proc. Natl. Acad. Sci. U.S.A 107, 16595e16600.
85. Capecchi, M.R., Pozner, A., 2015. ASPM regulates symmetric stem cell division by tuning Cyclin E ubiquitination. Nat. Commun. 6, 8763.
86. Bilgüvar, K., et al., 2010. Whole-exome sequencing identifies recessive WDR62 mutations in severe brain malformations. Nature 467, 207e210.
87. Yu, T.W., Mochida, G.H., Tischfield, D.J., Sgaier, S.K., Flores-Sarnat, L., Sergi, C.M., Topçu, M., McDonald, M.T., Barry, B.J., Felie, J.M., Sunu, C., Dobyns, W.B., Folkerth, R.D., Barkovich, A.J., Walsh, C.A., 2010. Mutations in WDR62, encoding a centrosome-associated protein, cause microcephaly with simplified gyri and abnormal cortical architecture. Nat. Genet. 42, 1015e1020.
88. Shohayeb, B., Lim, N.R., Ho, U., Xu, Z., Dottori, M., Quinn, L., Ng, D.C.H., 2018. The role of WD40-repeat protein 62 (MCPH2) in brain growth: diverse molecular and cellular mechanisms required for cortical development. Mol. Neurobiol. 55, 5409e5424.
89. Bogoyevitch, M.A., Yeap, Y.Y.C., Qu, Z., Ngoei, K.R., Yip, Y.Y., Zhao, T.T., Heng, J.I., Ng, D.C.H., 2012. WD40-repeat protein 62 is a JNK phosphorylated spindle pole protein required for spindle maintenance and timely mitotic progression. J. Cell Sci. 125, 5096e5109
90. Xu, D., Zhang, F., Wang, Y., Sun, Y., Xu, Z., 2014. Microcephaly-associated protein WDR62 regulates neurogenesis through JNK1 in the developing neocortex. Cell Rep. 6, 1176e1177.
91. Sgourdou, P., Mishra-Gorur, K., Saotome, I., Henagariu, O., Tüysüz, B., Campos, C., Ishigame, K., Giannikou, K., Quon, J.L., Sestan, N., Caglayan, A.O., Günel, M., Louvi, A., 2017. Disruptions in asymmetric centrosome inheritance and WDR62-Aurora kinase B interactions in primary microcephaly. Sci. Rep. 7, 43708.
92. Bianchi, F.T., Berto, G.E., Di Cunto, F., 2018. Impact of DNA repair and stability defects on cortical development. Cell. Mol. Life Sci. 75, 3963e3976.
93. Bicknell, L.S., Walker, S., Klingseisen, A., Stiff, T., Leitch, A., Kerzendorfer, C., Martin, C.-A., Yeyati, P., Sanna Al, N., Bober, M., Johnson, D., Wise, C., Jackson, A.P., O'Driscoll, M., Jeggo,

P.A., 2011b. Mutations in ORC1, encoding the largest subunit of the origin recognition complex, cause microcephalic primordial dwarfism resembling Meier-Gorlin syndrome. Nat. Genet. 43, 350e355.

94. Blackford, A.N., Jackson, S.P., 2017. ATM, ATR, and DNA-PK: the trinity at the heart of the DNA damage response. Mol. Cell 66, 801e817.
95. Shen, J., Gilmore, E.C., Marshall, C.A., Haddadin, M., Reynolds, J.J., Eyaid, W., Bodell, A., Barry, B., Gleason, D., Allen, K., Ganesh, V.S., Chang, B.S., Grix, A., Hill, R.S., Topçu, M., Caldecott, K.W., Barkovich, A.J., Walsh, C.A., 2010. Mutations in PNKP cause microcephaly, seizures and defects in DNA repair. Nat. Genet. 42, 245e249.
96. Genin, A., Désir, J., Lambert, N., Biervliet, M., Van Der Aa, N., Pierquin, G., Killian, A., Tosi, M., Urbina, M., Lefort, A., Libert, F., Pirson, I., Abramowicz, M., 2012. Kinetochore KMN network gene CASC5 mutated in primary microcephaly. Hum. Mol. Genet. 21, 5306e5317.
97. Mirzaa, G.M., Vitre, B., Carpenter, G., Abramowicz, I., Gleeson, J.G., Paciorkowski, A.R., Cleveland, D.W., Dobyns, W.B., O'Driscoll, M., 2014. Mutations in CENPE define a novel kinetochore-centromeric mechanism for microcephalic primordial dwarfism. Hum. Genet. 133, 1023e1039.
98. Takimoto, M., 2017. D40/KNL1/CASC5 and autosomal recessive primary microcephaly. Congenital. Anom. 57, 191e196.
99. D'Avino, P.P., 2017. Citron kinase- renaissance of a neglected mitotic kinase. J. Cell Sci. 130, 1701e1708.
100. Moawia, A., et al., 2017. Mutations of KIF14 cause primary microcephaly by impairing cytokinesis. Ann. Neurol. 82, 562e577.
101. Choi, Y.J., Anders, L., 2014. Signaling through cyclin D-dependent kinases. Oncogene 33, 1890e1903.
102. Barbelanne, M., Tsang, W.Y., 2014. Molecular and cellular basis of autosomal recessive primary microcephaly. BioMed Res. Int. 2014, 547986
103. Hussain, M.S., et al., 2013. CDK6 associates with the centrosome during mitosis and is mutated in a large Pakistani family with primary microcephaly. Hum. Mol. Genet. 22, 5199e5214.
104. Colasante, G., Simonet, J.C., Calogero, R., Crispi, S., Sessa, A., Cho, G., Golden, J.A., Broccoli, V., 2015. ARX regulates cortical intermediate progenitor cell expansion and upper layer neuron formation through repression of Cdkn1c. Cerebr. Cortex 25, 322e335.
105. Shoubridge, C., Fullston, T., Gécz, J., 2010. ARX spectrum disorders: making inroads into the molecular pathology. Hum. Mutat. 31, 889e900.
106. Reiner, O., Sapoznik, S., Sapir, T., 2006. Lissencephaly 1 linking to multiple diseases: mental retardation, neurodegeneration, schizophrenia, male sterility, and more. NeuroMolecular Med. 8 (4), 547e565.
107. Ghai, S., Fong, K.W., et al., 2006. Prenatal US and MR imaging findings of lissencephaly: review of fetal cerebral sulcal development. RadioGraphics 26 (2), 389e405.

108. Mochida, G.H., 2009. Genetics and biology of microcephaly and lissencephaly. Semin. Pediatr. Neurol. 16 (3), 120e126.
109. Spalice, A., Parisi, P., et al., 2009. Neuronal migration disorders: clinical, neuroradiologic and genetics aspects. Acta Paediatr. 98 (3), 421e433.
110. Di Donato N, Timms AE, Aldinger KA, Mirzaa GM, Bennett JT, Collins S, et al. Analysis of 17 genes detects mutations in 81% of 811 patients with lissencephaly. Genet Med 2018; 20: 1354–64.
111. Dobyns WB, Curry CJ, Hoyme HE, et al: Clinical and molecular diagnosis of Miller-Dieker syndrome. Am J Hum Genet 48:584-594, 1991.
112. Kerjan, G., Gleeson, J.G., 2007. Genetic mechanisms underlying abnormal neuronal migration in classical lissencephaly. Trends Genet. 23 (12), 623e630.
113. Jaglin, X.H., Chelly, J., 2009. Tubulin-related cortical dysgeneses: microtubule dysfunction underlying neuronal migration defects. Trends Genet. 25 (12), 555e566.
114. Pang, T., Atefy, R., Sheen, V., 2008. Malformations of cortical development. The Neurologist 14 (3), 181e191.
115. Okazaki, S., Ohsawa, M., et al., 2008. Aristaless-related homeobox gene disruption leads to abnormal distribution of GABAergic interneurons in human neocortex: evidence based on a case of X-linked lissencephaly with abnormal genitalia (XLAG). Acta Neuropathol. 116 (4), 453e462.
116. Valencia, C.A., Pervaiz, M.A., Husami, A., Qian, Y., Zhang, K. (2013). Sanger Sequencing Principles, History, and Landmarks. In: Next Generation Sequencing Technologies in Medical Genetics. SpringerBriefs in Genetics. Springer, New York, NY.
117. Hutchison CA 3rd (2007) DNA sequencing: bench to bedside and beyond. Nucleic Acids Res 35:6227–6237.
118. Shendure JA, Porreca GJ, Church GM et al (2011) Overview of DNA sequencing strategies. In: FM Ausubel et al (ed) Curr Protoc Mol Biol, Chapter 7, Unit 7.1. John Wiley & Sons, Inc.
119. Smith LM et al. (1986) Fluorescence detection in automated DNA sequence analysis. Nature 321:674–679.
120. Ju J, Glazer AN, Mathies RA (1996) Energy transfer primers: a new fluorescence labeling paradigm for DNA sequencing and analysis. Nat Med 2:246–249.
121. Smith, L.M., Kaiser, R.J., Sanders, J.Z., and Hood, L.E. 1987. The synthesis and use of fluorescent oligonucleotides in DNA sequence analysis. Methods Enzymol. 155: 260–301.
122. Ewing, B., Hillier, L., Wendl, M.C., and Green, P. 1998. Base-calling of automated sequencer traces using Phred. I. Accuracy assessment. Genome Res. 8: 175–185.
123. Dressman, D., Yan, H., Traverso, G., Kinzler, K. W. & Vogelstein, B. Transforming single DNA molecules into fluorescent magnetic particles for detection and enumeration of genetic variations. Proc. Natl. Acad. Sci. USA 100, 8817–8822 (2003).
124. Fedurco, M., Romieu, A., Williams, S., Lawrence, I. & Turcatti, G. BTA, a novel reagent for DNA attachment on glass and efficient generation of solid-phase amplified DNA colonies. Nucleic Acids Res. 34, e22 (2006).

125. Korlach, J., Marks, P. J., Cicero, R. L., Gray, J. J., Murphy, D. L., Roitman, D. B., Pham, T. T., Otto, G. A., Foquet, M., & Turner, S. W. (2008). Selective aluminum passivation for targeted immobilization of single DNA polymerase molecules in zero-mode waveguide nanostructures. *Proceedings of the National Academy of Sciences of the United States of America*, *105*(4), 1176–1181.
126. Fan, J.-B., Chee, M. S. & Gunderson, K. L. Highly parallel genomic assays. Nature Rev. Genet. 7, 632–644 (2006).
127. Metzker, M. L. Emerging technologies in DNA sequencing. Genome Res. 15, 1767–1776 (2005).
128. Wu, W., Litosh, V. A., Stupi, B. P. & Metzker, M. L. Photocleavable labeled nucleotides and nucleosides and methods for their use in DNA sequencing. US Patent Application 11/567,189 (2009).
129. Bowers, J. et al. Virtual terminator nucleotides for next-generation DNA sequencing. Nature Methods 6, 593–595 (2009).
130. Braslavsky, I., Hebert, B., Kartalov, E. & Quake, S. R. Sequence information can be obtained from single DNA molecules. Proc. Natl. Acad. Sci. USA 100, 3960–3964 (2003).
131. Ronaghi, M., Uhlén, M. & Nyrén, P. A sequencing method based on real-time pyrophosphate. Science 281, 363–365 (1998).
132. Margulies, M. et al. Genome sequencing in microfabricated high-density picolitre reactors. Nature 437, 376–380 (2005).
133. Levene, M. J. et al. Zero-mode waveguides for single molecule analysis at high concentrations. Science 299, 682–686 (2003).
134. Valouev, A. et al. A high-resolution, nucleosome position map of C. elegans reveals a lack of universal sequence-dictated positioning. Genome Res. 18, 1051–1063 (2008).
135. Pareek, C. S., Smoczynski, R., & Tretyn, A. (2011). Sequencing technologies and genome sequencing. *Journal of applied genetics*, *52*(4), 413–435.
136. Yang Y, Muzny DM, Xia F, et al. Molecular findings among patients referred for clinical whole-exome sequencing. JAMA 2014;312:1870–1879.
137. Li H. (2013) Aligning sequence reads, clone sequences and assembly contigs with BWA-MEM. arXiv:1303.3997v2 [q-bio.GN].
138. DePristo M, Banks E, Poplin R, Garimella K, Maguire J, Hartl C, Philippakis A, del Angel G, Rivas MA, Hanna M, McKenna A, Fennell T, Kernytsky A, Sivachenko A, Cibulskis K, Gabriel S, Altshuler D, Daly M. (2011). A framework for variation discovery and genotyping using next-generation DNA sequencing data. Nat Genet, 43:491-498.
139. Cingolani, P., Platts, A., Wang, leL., Coon, M., Nguyen, T., Wang, L., Land, S. J., Lu, X., & Ruden, D. M. (2012). A program for annotating and predicting the effects of single nucleotide polymorphisms, SnpEff: SNPs in the genome of Drosophila melanogaster strain w1118; iso-2; iso-3. *Fly*, *6*(2), 80–92.
140. Wang, K., Li, M., & Hakonarson, H. (2010). ANNOVAR: functional annotation of genetic variants from high-throughput sequencing data. *Nucleic acids research*, *38*(16), e164.

141. McLaren, W., Gil, L., Hunt, S.E. *et al.* The Ensembl Variant Effect Predictor. *Genome Biol* **17**, 122 (2016).
142. McKusick, V.A.: Mendelian Inheritance in Man. A Catalog of Human Genes and Genetic Disorders. Baltimore: Johns Hopkins University Press, 1998 (12th edition).
143. Chen, S., Francioli, L.C., Goodrich, J.K. *et al.* A genomic mutational constraint map using variation in 76,156 human genomes. *Nature* **625**, 92–100 (2024).
144. Bycroft, C., Freeman, C., Petkova, D. *et al.* The UK Biobank resource with deep phenotyping and genomic data. *Nature* **562**, 203–209 (2018).
145. The 1000 Genomes Project Consortium. A global reference for human genetic variation. *Nature* 526, 68–74 (2015).
146. Glusman, G., Caballero, J., Mauldin, D. E., Hood, L., & Roach, J. C. (2011). Kaviar: an accessible system for testing SNV novelty. *Bioinformatics (Oxford, England)*, *27*(22), 3216–3217.
147. Fattahi Z, Beheshtian M, Mohseni M, Poustchi H, Sellars E, Nezhadi SH, Amini A, Arzhangi S, Jalalvand K, Jamali P, Mohammadi Z, Davarnia B, Nikuei P, Oladnabi M, Mohammadzadeh A, Zohrehvand E, Nejatizadeh A, Shekari M, Bagherzadeh M, Shamsi-Gooshki E, Börno S, Timmermann B, Haghdoost A, Najafipour R, Khorram Khorshid HR, Kahrizi K, Malekzadeh R, Akbari MR, Najmabadi H. Iranome: A catalog of genomic variations in the Iranian population. Hum Mutat. 2019 Nov;40(11):1968-1984.
148. Richards S, Aziz N, Bale S, Bick D, Das S, Gastier-Foster J, et al. Standards and guidelines for the interpretation of sequence variants: a joint consensus recommendation of the American College of Medical Genetics and Genomics and the Association for Molecular Pathology. Genet Med. 2015;17(5):405-24.
149. Kent WJ, Sugnet CW, Furey TS, Roskin KM, Pringle TH, Zahler AM, Haussler D. The human genome browser at UCSC. Genome Res. 2002 Jun;12(6):996-1006.
150. PrimerQuest™ program, IDT, Coralville, Iowa, USA. Accessed 12 December, 2018.
151. Talevich, E., Shain, A. H., Botton, T., & Bastian, B. C. (2016). CNVkit: Genome-Wide Copy Number Detection and Visualization from Targeted DNA Sequencing. *PLOS Computational Biology*, *12*(4), e1004873.
152. Chen, X., Schulz-Trieglaff, O., Shaw, R., Barnes, B., Schlesinger, F., Källberg, M., Cox, A. J., Kruglyak, S., & Saunders, C. T. (2015). Manta: rapid detection of structural variants and indels for germline and cancer sequencing applications. *Bioinformatics*, *32*(8), 1220–1222.
153. Geoffroy, V., Lamouche, J. B., Guignard, T., Nicaise, S., Kress, A., Scheidecker, S., Le Béchec, A., & Muller, J. (2023). The AnnotSV webserver in 2023: updated visualization and ranking. *Nucleic acids research*, *51*(W1), W39–W45.
154. Chang CC, Chow CC, Tellier LCAM, Vattikuti S, Purcell SM, Lee JJ (2015) Second-generation PLINK: rising to the challenge of larger and richer datasets. GigaScience,4.
155. Divina, P., Kvitkovicova, A., Buratti, E., & Vorechovsky, I. (2009). Ab initio prediction of mutation-induced cryptic splice-site activation and exon skipping. *European journal of human genetics : EJHG*, *17*(6), 759–765.

156. Hwang, J., & Kim, Y. K. (2013). When a ribosome encounters a premature termination codon. *BMB reports*, *46*(1), 9–16.

157. Poirier, K., Martinovic, J., Laquerrière, A., Cavallin, M., Fallet-Bianco, C., Desguerre, I., Valence, S., Grande-Goburghun, J., Francannet, C., Deleuze, J. F., Boland, A., Chelly, J., & Bahi-Buisson, N. (2015). Rare ACTG1 variants in fetal microlissencephaly. *European journal of medical genetics*, *58*(8), 416–418.

158. Houlard, M., Cutts, E. E., Shamim, M. S., Godwin, J., Weisz, D., Presser Aiden, A., Lieberman Aiden, E., Schermelleh, L., Vannini, A., & Nasmyth, K. (2021). MCPH1 inhibits Condensin II during interphase by regulating its SMC2-Kleisin interface. *eLife*, *10*, e73348.

159. Levy, M. A., Fernandes, A. D., Tremblay, D. C., Seah, C., & Bérubé, N. G. (2008). The SWI/SNF protein ATRX co-regulates pseudoautosomal genes that have translocated to autosomes in the mouse genome. *BMC genomics*, *9*, 468.

160. Cavalcante, L. A., Garcia-Abreu, J., Mendes, F. A., Moura Neto, V., Silva, L. C., Onofre, G., Weissmüller, G., & Carvalho, S. L. (2003). Sulfated proteoglycans as modulators of neuronal migration and axonal decussation in the developing midbrain. *Brazilian journal of medical and biological research = Revista brasileira de pesquisas medicas e biologicas*, *36*(8), 993–1002.

161. Maeda N. (2015). Proteoglycans and neuronal migration in the cerebral cortex during development and disease. *Frontiers in neuroscience*, *9*, 98.

162. Olson, H. E., Jean-Marçais, N., Yang, E., Heron, D., Tatton-Brown, K., van der Zwaag, P. A., Bijlsma, E. K., Krock, B. L., Backer, E., Kamsteeg, E. J., Sinnema, M., Reijnders, M. R. F., Bearden, D., Begtrup, A., Telegrafi, A., Lunsing, R. J., Burglen, L., Lesca, G., Cho, M. T., Smith, L. A., Thauvin-Robinet, C. (2018). A Recurrent De Novo PACS2 Heterozygous Missense Variant Causes Neonatal-Onset Developmental Epileptic Encephalopathy, Facial Dysmorphism, and Cerebellar Dysgenesis. *American journal of human genetics*, *102*(5), 995–1007.

163. Dekker, J., Diderich, K. E. M., Schot, R., Husen, S. C., Dremmen, M. H. G., Go, A. T. J. I., Weerts, M. J. A., van Slegtenhorst, M. A., & Mancini, G. M. S. (2021). A novel family illustrating the mild phenotypic spectrum of TUBB2B variants. *European journal of paediatric neurology : EJPN : official journal of the European Paediatric Neurology Society*, *35*, 35–39.

164. Yang Y, Muzny DM, Xia F et al: Molecular findings among patients referred for clinical whole-exome sequencing. JAMA 2014; 312: 1870–1879.

165. Makrythanasis P, Nelis M, Santoni FA et al: Diagnostic exome sequencing to elucidate the genetic basis of likely recessive disorders in consanguineous families. Hum Mutat 2014; 35: 1203–1210.

166. Bortolami, A., Yu, W., Forzisi, E., Ercan, K., Kadakia, R., Murugan, M., Fedele, D., Estevez, I., Boison, D., Rasin, M. R., & Sesti, F. (2023). Integrin-KCNB1 potassium channel complexes regulate neocortical neuronal development and are implicated in epilepsy. *Cell death and differentiation*, *30*(3), 687–701.

167. Moreno-Layseca, P., & Streuli, C. H. (2014). Signalling pathways linking integrins with cell cycle progression. *Matrix biology : journal of the International Society for Matrix Biology*, *34*, 144–153.

168. Cooper, J., & Giancotti, F. G. (2019). Integrin Signaling in Cancer: Mechanotransduction, Stemness, Epithelial Plasticity, and Therapeutic Resistance. *Cancer cell*, *35*(3), 347–367.

8 APPENDIX

APPENDIX 1. Ethics Committee Decision

APPENDIX 1. Ethics Committee Decision (continued)

APPENDIX 1. Ethics Committee Decision (continued)

9 CURRICULUM VITAE